UNIVERSIDADE FEDERAL DE SANTA CATARINA
CENTRO TECNOLÓGICO DE JOINVILLE
CURSO DE ENGENHARIA AEROESPACIAL

RICARDO BITTENCOURT

PRELIMINARY THERMAL MANAGMENT DESIGN OF A 6U CUBESAT WITH A HIGH POWER R-LEMA LASER EXPERIMENT PAYLOAD

Joinville
2022

RICARDO BITTENCOURT

PRELIMINARY THERMAL MANAGMENT DESIGN OF A 6U CUBESAT WITH A HIGH POWER R-LEMA LASER EXPERIMENT PAYLOAD

Trabalho apresentado como requisito para obtenção do título de bacharel em Engenharia Aeroespacial do Centro Tecnológico de Joinville da Universidade Federal de Santa Catarina.

Orientador: Dr. Kleber de Paiva

Coorientador: Dr. Gary B. Hughes

Joinville
2022

RICARDO BITTENCOURT

PRELIMINARY THERMAL MANAGMENT DESIGN OF A 6U CUBESAT WITH A HIGH POWER R-LEMA LASER EXPERIMENT PAYLOAD

Este Trabalho de Conclusão de Curso foi julgado adequado para obtenção do título de bacharel em Engenharia Aeroespacial, na Universidade Federal de Santa Catarina, Centro Tecnológico de Joinville.

Joinville (SC), 14 de Fevereiro de 2022.

Examining board:

_____

Orientador: Dr. Kleber de Paiva
Orientador(a)
Presidente

_____

Prof. Dr.Talita Possamai
Membro
Universidade Federal de Santa Catarina

_____

Prof. Dr. Gary Hughes
Membro
University of California Santa Barbara

Dedico este trabalho à colonização humana do Sistema Solar

ACKNOWLEDGMENT

Ao meu orientador, Kleber Vieira Paiva, pela atenção e confiança.
Ao professor Gary B. Hughes, pela oportunidade de participar do projeto NIAC e de todo o apoio durante o estágio na California Polytechnic State University.

ABSTRACT

This work describes thermal analysis of a standard 6U Cubesat whose mission is to carry out tests of Remote Laser Evaporative Molecular Absorption (R-LEMA) spectroscopy, a concept developed under the NASA Innovative Advanced project Concepts (NIAC) program. A conceptual R-LEMA satellite utilizes a 200 W laser, which is 50% efficient. An experiment is performed by firing the laser for 20 seconds, while generating 200 W of waste heat during the active period; the waste heat must then must be dissipated prior to the next laser firing. In order to manage the heat generated by the laser, a 0.06 m^2 radiator and a Phase Change Material (PCM) block of 100 g of Polyethylene glycol are simulated. A Thermal Mathematical Model is developed for the 6U CubeSat frame with representative R-LEMA components, taking into account several nodes which are treated as clustered systems. The analysis is done through the explicit numerical method of finite differences to obtain graphs of the transient simulation of temperatures of the laser, satellite bus, and of the radiator. From the results, it was concluded that the radiator alone provides thermal management which is sufficient to perform one test per orbit, i.e., a experiments can be conducted at a cadence of 90 minutes, without significant heat accumulation in the spacecraft components. Addition of the PCM allowed the storage of heat of fusion from waste heat, and allowed a cadence of 5 minutes.

Keywords: Cubesat 6U. Nanosatellite. Thermal Control. Laser. Spectrometer.

RESUMO

O Modelo Matemático Térmico de um nanossatélite leva em consideração vários nós que são tratados como sistemas aglomerados. Neste trabalho, um satélite padrão Cubesat 6U que tem como missão realizar testes de Remote Laser Evaporative Molecular Absorption (R-LEMA) para um projeto da NASA Innovative Advanced Concepts (NIAC) é analisado. Este projeto desenvolve um conceito que permite detectar, através do espectrômetro, a composição de alvos frios do sistema solar a partir de um laser que esquenta tal alvo. O experimento com Laser R-LEMA é executado por 20 segundos produzindo 200W de excesso de calor a ser administrado. A fim de administrar o calor gerado pelo experimento R-LEMA, um radiador de 0.06m² e um bloco de Phase Change Material (PCM) do 100 g de Polyethylene glycol são simulados. A análise é feita através do método numérico explícito das diferenças finitas para obter gráficos da simulação do transiente de temperaturas do laser, bus do satélite e do radiador. Dos resultados, concluiu-se que o radiador sozinho é suficiente para administrar o calor caso realiza-se um teste por órbita, no entanto, o PCM mostrou-se útil ao permitir a realização de mais de um teste por órbita a uma cadencia de 5 minutos.

Palavras-chave: Cubesat 6U. Nanossatélite. Controle Térmico. Laser. Espectrômetro.

LIST OF FIGURES

LIST OF TABLES

LIST OF SYMBOLS

$\dot{Q}$	Rate of net heat transfer
k	Thermal Conductivity
A	Area
h	convection heat transfer coefficient
T_s	Surface temperature
$T_{\inf}$	Ambient temperature
T_{sur}	Surroundings temperature
T_i	Temperature of node i
σ	Stefan-Boltzmann constant
ε	Emissivity
η	Solar cell efficiency
F	Form factor
t	Time
m	Mass
c	Specific heat
C	Heat mass

TABLE OF CONTENTS

1 INTRODUCTION

Thermal Control is an important aspect in the development of satellites, as it is crucial to keep all components in their various ranges of operating temperatures. As a result, to meet the thermal limitations of the spacecraft components at all stages of the mission (pre- launch, launch or operational flight in various scenarios), a system of thermal control should be designed in such a way as to manage the heat flow within, to and spacecraft (PISACANE, 2008).

According to Meseguer, Grande and Andres (2012), the first step towards determine the set of variables related to the design of this complex system, by the classical approach, is to define the mission in a generic way. The second step is define all secondary mission objectives as well as limitations and restrictions. Several mission factors, placed side by side, generate a basis on which the system thermal control can be defined in a way that meets all requirements and restrictions, such as cost, size, and performance.

This work was carried out in partnership with a academic work sponsored by NASA Innovative Advanced Conceps (NIAC). NIAC is a NASA program looking for innovative concepts to revolutionize the aerospace industry.

> The NASA Innovative Advanced Concepts (NIAC) Program nurtures visionary ideas that could transform future NASA missions with the creation of breakthroughs — radically better or entirely new aerospace concepts — while engaging America's innovators and entrepreneurs as partners in the journey.al. The program seeks innovations from diverse and non-traditional sources and NIAC projects study innovative, technically credible, advanced concepts that could one day "change the possible" in aerospace. (NASA INNOVATIVE ADVANCED CONCEPTS, 2021).

Within this context, the goal of academic work is to develop a space probe to analyze the composition of cold objects in the solar system (comets, asteroids, planets and moons) from a distant point. Such information is critical to understanding the formation and origin of the solar system as well as expanding human knowledge about space, enabling missions to diverge asteroids with high chances of impact with Earth, in addition to other advances.

The concept of the mission, illustrated in Figure 1, is understood to focus on a laser energy beam at a small point on the surface of the object, so the material melts and evaporates. The ejected steam retains the composition of the material, since the laser energy is not sufficient for ionization, the material is, then illuminated by the black body radiation emitted by the heated point. Absorptions molecular and atomic effects happen as radiation passes through the plume of material which in turn can be investigated by a

spectrometer pointed at the heating point through the steam plume (HUGHES; LUBIN, 2017). Hughes and Lubin also explain that:

> The diagram (Figure 1) shows a spacecraft orbiting an asteroid. [...]. The diagram illustrates laser beams emanating from each element in the laser array. The laser beams emanating from the laser array converge on an asteroid that is apparently located at a significant distance from the spacecraft. The distant asteroid appears as a rocky body, and there is an indication that the focused laser beams are heating a spot on the asteroid's surface. A diffuse plume of evaporated material is depicted near the asteroid, around the area of the heated spot. (p. 8).

Figure 1 – A System for Probing the Molecular Composition of Cold Solar System Targets, such as Asteroids, Comets, Planets and Moons, from a Distant Vantage, e.g. from Orbit around the Target.

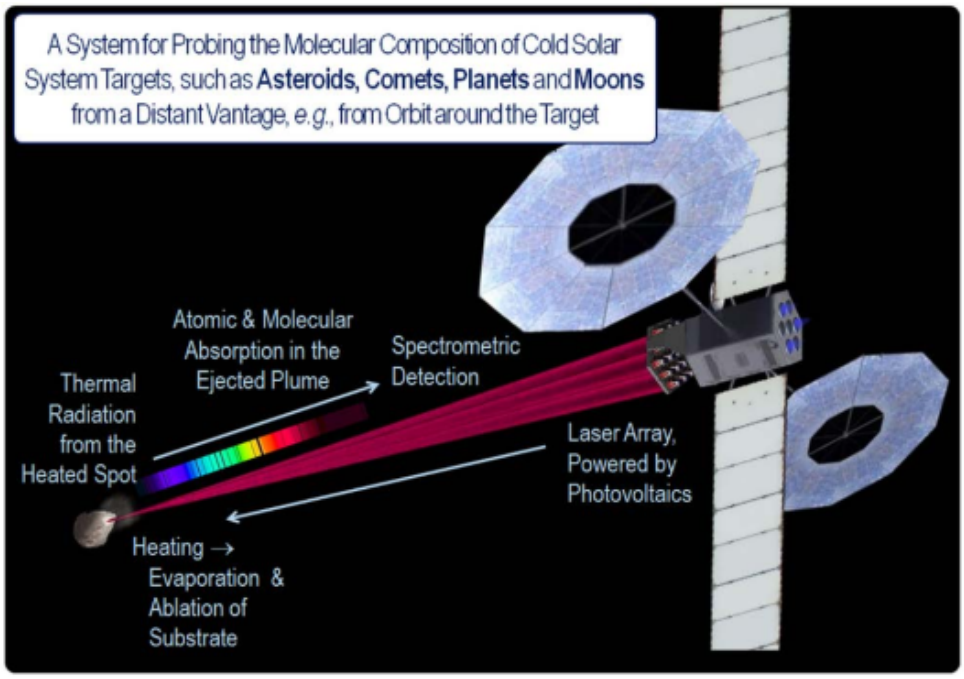

Credit:Hughes e Lubin (2017, p. 8).

The mission addressed by this work, however, is a mission of proof of concept, i.e. a smaller-scale mission conducted in order to demonstrate the feasibility and uncover possible challenges with regard to the completion of the final spacecraft. It consists of a smaller scale laser ($\approx 200W$) mounted on a CubeSat 6U nanosatellite (10cm x 30cm x 20cm), which heats up a point in an artificial rock sample released in nearby. With this, one can get answers to the inquiries suggested by Meseguer et al (2012) and Pisacane (2008).

The mission, in a general way, is a test mission, but in a way that it is a space vehicle that will activate a high waste heat generation component (Laser), periodically while traveling through a low Earth orbit . With that mission in mind, one can consider

laser an element of high interest for the thermal control project, since it is the component of the spacecraft that generates most heat while it is activated.

The importance of laser is given by the fact that all systems of the satellite must be within their respective operating temperature range and, as proposed by Gilmore (2002), the environment of the low Earth orbit has greater incidence of radiation from albedo and emission of infrared radiation by the Earth, in addition to solar radiation itself making it difficult to eliminate the internal heat of the spacecraft. It is noteworthy that, in the vacuum of space, thermal conditions change drastically in short periods and the absence of air prevents heat exhaustion from the laser through convection, this further complicates thermal control (ÇENGEL; GHAJAR, 2009).

1.1 OBJECTIVE

To facilitate the development of a thermal control system suitable for the nanossatellite, the following objectives are proposed in this work.

1.1.1 General Objective

To develop a preliminary thermal model of a high power laser and alternatives for the thermal control system in a 6U cubesat.

1.1.2 Specific Objectives

- Obtain the necessary considerations and hypotheses for the thermal design;
- Obtain the equations of the Thermal Mathematical Model (TMM)
- Investigate the impact of using PCM and heat pipes in temperature control.

2 LITERATURE AND TECHNOLOGY SURVEY

In this chapter will be presented the theories of thermodynamics and heat transfer necessary to describe the methodology of this work. It will also be introduced technologies in their state of the art considered essential for thermal control of small satellites. The equations presented will be used for the mathematical modeling in the methodology of this study.

2.1 ENERGY TRANSFER

There are two ways to transfer energy. Heat Transfer and Work. Energy transfer is considered work when it is not an influence of the temperature difference (ÇENGEL; GHAJAR, 2009). In this work, the only type of energy transfer studied is the transfer of thermal energy, i.e. of heat. Heat can be transferred in three ways: conduction, convection and radiation.

2.2 HEAT TRANSFER

Çengel and Ghajar (2009) explainin that: "The science of thermodynamics deals with the amount of heat transfer as a system undergoes a process from one equilibrium state to another, and makes no reference to how long the process will take. "(ÇENGEL; GHAJAR, 2009, p. 2). Still according to Çengel and Ghajar (2009), heat is defined as a form of energy from which its potential for movement is temperature differential. The Science of heat transfer studies the transfer rates of this type of energy.

2.2.1 Conduction

Conduction is the most common means of heat transfer in everyday life, and therefore the most intuitive. According to Çengel and Ghajar (2009), conduction is the transfer of energy from particles through their interactions through vibrations of the Molecules. Conduction occurs in materials of any phase: solid, liquid or gaseous, however, in liquids and gases conduction occurs due to molecular shocks, and in solids, it occurs due to the vibrations of adjacent molecules. Conduction is modelled by the Fourier Law, which was postulated in 1822 by Jean Baptiste Joseph Fourier (Equation 1).

$$\dot{Q}_{cond} = -kA\frac{dT}{dx} \tag{1}$$

Equation 1 indicates that the heat transfer rate ($\dot{Q}$) is directly proportional to the thermal conductivity of the material (k), the contact area (A) and the temperature difference (dT) and which is inversely proportional to the thickness of the material (dx).

In satellites and Cubesats conduction is present in the heat transfer between the internal components of the spacecraft and also between them and the structure where there are direct contacts such as flanges, washers and screws. (GILMORE, 2002).

2.2.2 Convection

For Çengel and Ghajar (2009), convection is the mode of transfer of heat that occurs at the interface between solids and fluids. This heat transfer is characterized by fluid movement. If there is no movement of the fluid, then it is of pure conduction. Convection is modeled through Newton's Law of Cooling (Equation 2):

$$\dot{Q}_{conv} = hA(T_s - T_\infty) \tag{2}$$

Where h is the convection heat transfer coefficient ($W/m^2 \cdot K$). This coefficient is experimentally determined and summarizes all the variables that influence the process, such as surface geometry, nature of fluid movement, fluid properties, etc. Like conduction, convection also depends on the temperature difference between the surface (T_s) and the fluid at a distance (T_∞). This type of conduction depends on a gaseous medium, which is rare in the environment of a satellite, so it will not be addressed in this work.

2.2.3 Radiation

Radiation is the form of energy transferred through electromagnetic waves. This is the only way that does not depend on an intervening means for it to occur. Actually, heat transfer by radiation is faster in the vacuum, where there is no particles to attenuate such a phenomenon. (ÇENGEL; GHAJAR, 2009). The maximum rate of radiation heat transfer from a surface with temperature (T_s) is calculated by stefan-Boltzmann's law of thermal radiation, given by Equation 3.

$$\dot{Q}_{rad_{max}} = \sigma A_s T_s^4 \tag{3}$$

where $\sigma = 5,670 \times 10^{-8} W/m^2 \cdot K^4$ is stefan-boltzmann's constant. The energy rate emitted is a theoretical maximum amount called the black body radiation. The actual surfaces have a lower rate, quantified by multiplying the previous equation by ε, the emissivity. The emissivity is in the range of $0 \leq \varepsilon \leq 1$, and for $\varepsilon = 1$, it has black body

radiation. The rate of heat transmission between two surfaces can be obtained through energy conservation and is determined by Equation 4:

$$\dot{Q}_{rad} = \varepsilon \sigma A_s (T_s^4 - T_{sur}^4) \tag{4}$$

Where T_{sur} represents the temperature of the vicinity of surface S or another surface that exchanges heat with it.

For an orbiting spacecraft, thermal radiation is the main and majority means of heat transfer to and from the environment. (MESEGUER; GRANDE; ANDRES, 2012).

2.3 SPACE ENVIROMMENT

The space environment, with regard to thermal control of a spacecraft, is dominated by three forms of heating: solar radiation, planetary radiation, and radiaton reflected on the nearest planet, called albedo. (GILMORE, 2002). For Pisacane (2008), there is still deep space radiation (3K) and radiation reabsorbed from other parts of the satellite. Radiation is the main mean of heat transfer, since in space there is no atmosphere, however, in some cases, the energy of free molecules or molecular flows may be a heat source for the vehicle. (GILMORE, 2002). Thermal control is achieved through the balance of the energy emitted by the satellite and its radiators and the absorbed through the means mentioned above. The forms of heat inlet and outlet of the spacecraft are represented in Figure 2.

Figure 2 – Simplified scheme heat transfer of a spacecraft orbiting the earth

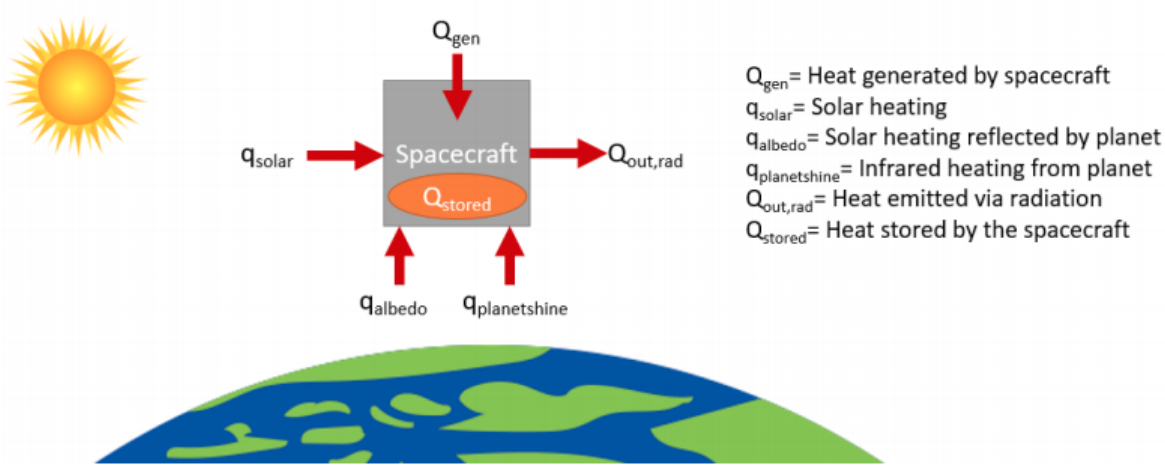

Credit: NASA (2021, p. 183).

2.3.1 Direct solar radiation

Direct solar radiation is the largest source of heat in space, a very stable source of radiation. During the 11 year solar cycle, it varies by 1%. However, due to the eccentricity of the Earth's orbit, the incident rate on the planet ranges from $1322W/m^2$ to $1414W/m^2$. The most used and recommended value is the average of the previous values: $1367W/m^2$ (GILMORE, 2002).

2.3.2 Albedo

"Albedo is defined as the amount of electromagnetic radiation reflected from a surface to the amount of energy incident on it."(PISACANE, 2008, p. 60). According to Gilmore (2002), albedo can be the product of the reflection of solar energy on a planet or moon and is usually a fraction of this energy. It can vary greatly depending on the type of planetary surface that reflects radiation, angle of reflection, and cloud cover.

2.3.3 Planetary IR radiation

The radiation emitted by planets is the heat emission linked to the temperature of the surface, which on average is considered 18 degrees Celsius. It depends on variables similar to the albedo ones, however, this radiation deals with heat emission absorbed by the earth's surface therefore occurs even during the dark phase of orbit. Because it is not an electromagnetic energy with short wavelengths as the energy emitted by the sun this type of energy cannot be reflected with coatings on radiators, as coatings for these wavelengths would prevent the radiator from operate (GILMORE, 2002)

2.3.4 Temperature of the cosmic microwave background

Fixsen (2009) obtained a cosmic microwave background temperature value of 2.7260 ± 0.0013 Kelvin. For the remainder of this work the space will be considered a surface at constant temperature and will be adopted the nearest integer value of 3 Kelvin.

2.4 CUBESATS

The term Cubesat refers to a pico-satellite standard developed in 1999 by J. Puig-Suari of the Polytechnic University of California in San Luis Obispo and Robert Twiggs of Stanford University, California in order to ensure access to universities and amateur projects to the space environment, enabling so low-cost experiments in earth's orbit. (NASA, 2021). The Cubesat standard is defined by the class of satellites that can be ejected by systems known as P-PODs (Figure 3), which have several models

designed to launch up to 12U. (SWARTWOUT, 2013). Cubesats have a form factor known as U, each 1U corresponds to a 10cm x 10cm x 10cm cube with mass of approximately 1kg, the most common Cubesats configurations are shown in Figure 4. The basic design of the satellite is composed of a structure with a stack of circuit boards inside. Each face of the satellite is covered with power panels. (HEIDT et al., 2000). The Cubesat studied in this work is one of the 6U standard, with approximately 30cm x 20cm x 10cm.

Figure 3 – P-POD releasing CubeSats 1U with detail on the rails

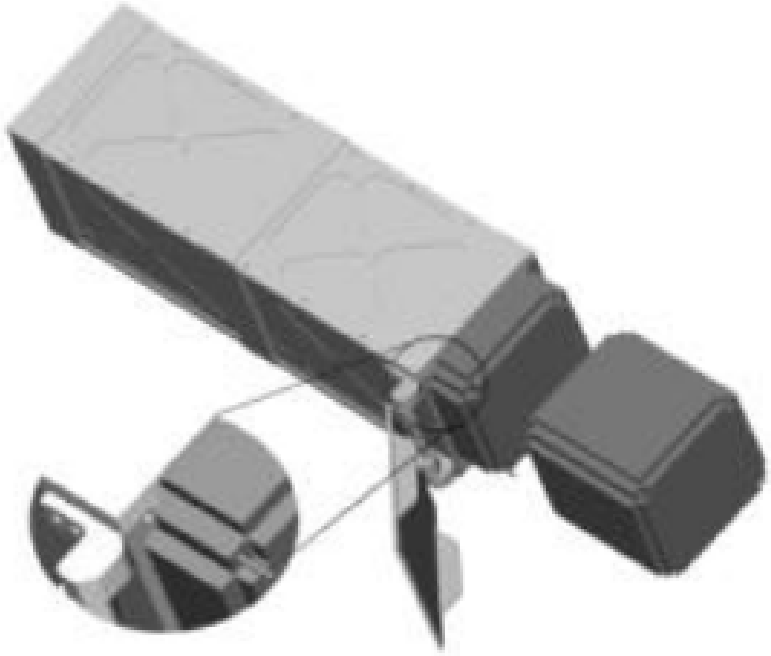

Credit: Heidt et al. (2000, p. 8).

Figure 4 – CubeSats are a class of nano- and microsatellites that use a standard size and form factor

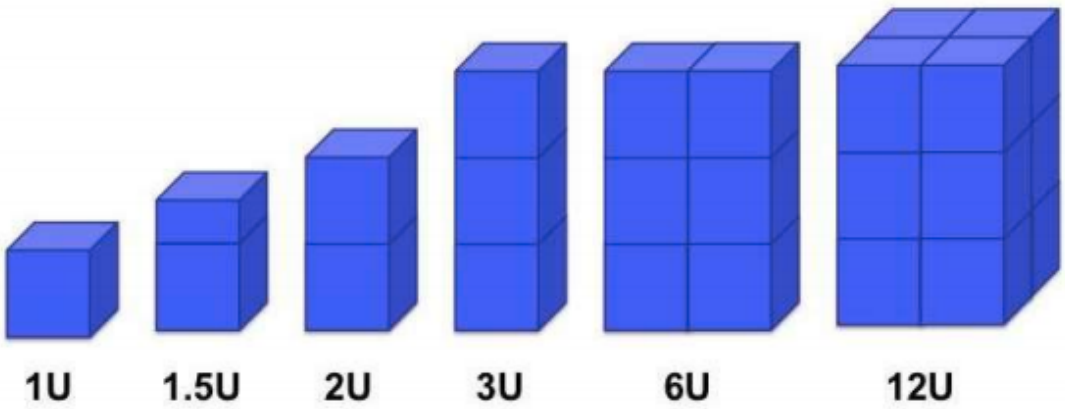

Credit: NASA (2021, p. 2).

2.5 THEARMAL CONTROL IN CUBESATS

Temperatures in a spacecraft are controlled by two types of thermal control: active and passive. Many of the methods used in large satellites are applicable in Cubesats, However, new challenges arise when applying such technologies miniaturized satellites. (NASA, 2021). The main challenges, such as proposed in the NASA report are:

- **Low thermal mass:** The spacecraft is more reactive to changing thermal environments.
- **Limited external surface area:** There is less real estate to be allocated to solar cells, designated radiator area, and/or viewports required for science instruments.
- **Limited volume:** There is less space for electronic components, science instruments, and thermal control hardware. Components can be more thermally coupled.
- **Limited power:** There is less power available for powered thermal control technology.

The main methods of thermal control with technological advances in the state of the art aimed at small satellites and Cubesats will be briefly described.

2.5.1 Passive Systems

Passive thermal control systems are the cheapest and involve little risk, since it does not consume energy, has no moving parts, is light and occupies little space. Passive systems are exemplified by Multi Layer Insulation (MLI), paints, coatings, sunshields, heat pipes, thermal straps and others. (NASA, 2021).

2.5.1.1 Paints, Coatings, and Tapes

In space, the only forms of heat transfer are conduction and radiation. To ensure thermal control of the spacecraft, one can add finishing to its surfaces such as films and adhesive tapes in order to change its emissivity and absorptivity properties of radiation. For example, a black matte surface has high absorption and radiation emission capacity, while a white epoxy paint has high emissivity and low solar radiation absorption, ideal for radiators or components that need to release heat. (NASA, 2021). According to Gilmore (2002), to minimize both absorption and emission of infrared energy, gold, silver or aluminum foil finishes are used in modern spacecraft. Typical values of absorptivity (α) and emissivity (ε) for different types of coatings are shown in Figure 5.

Figure 5 – Surface properties of coating materials

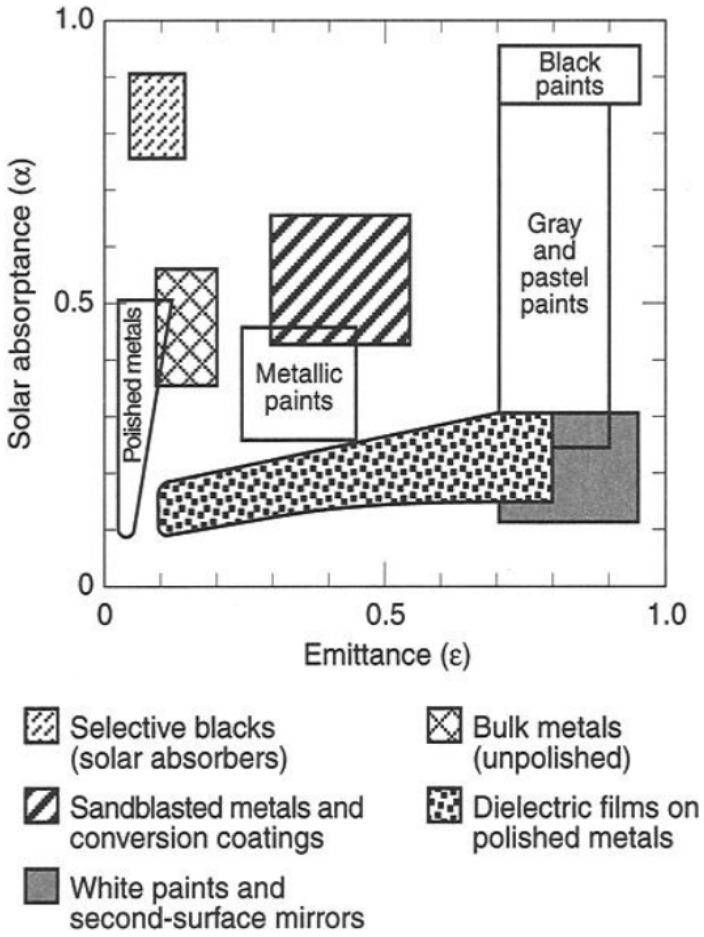

Credit: Gilmore (2002, p. 141).

2.5.1.2 Multi Layer Insulation

Generally, Multi Layer Insulation is a type of high performance insulator which uses various anti-conduction and radiation barriers ranging from several designs. (FINCKENOR, 1999). They are composed of several layers of films with low emissivity constructed with embossed Mylar sheets with a finish of vacuum deposition of aluminum or gold. As a result of the embossing method, layers touch in a few points, ensuring an isolation of heat conduction. (GILMORE, 2002). MLIs confer low performance when compressed, caused by by the high conductance of the layers in contact, therefore should be avoided outside cubesats where there will be degradation of the material at the point of contact with the P-POD. (NASA, 2021). In Figure 6, Finckenor demonstrates a construction scheme of an MLI blanket.

Figure 6 – Schematic cross section depicts the key elements of an MLI blanket. Not all elements need be present in every design.

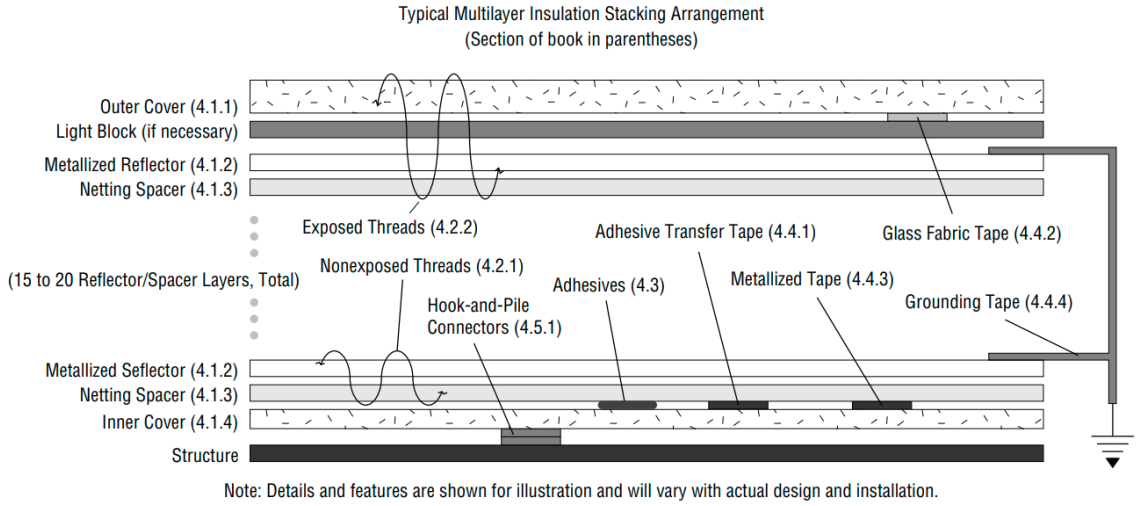

Credit: Finckenor (1999, p. 1).

2.5.1.3 Thermal straps and heat pipes

Thermal straps are a flexible type of heat conductor made of copper, aluminum or graphite that are typically used to transfer heat from a component generator to the Chassis of the Cubesat, a radiator or other surface that act as a heatsink. (NASA, 2021).

Heat pipes act in a similar manner, however, have a porous inner cavity partially filled a fluid that evaporates at the hot side and liquidises on the cold side of the tube. The liquid returns to the hot side of the tube through capillary action. (NASA, 2021). Figure 7 shows a heat pipe installed in a Cubesat 1U next to a heat pipe ready to be Installed.

2.5.1.4 Sunshields

Sunshields are "[...] an often deployed device made up of a material with low solar absorptivity that reduces the amount of incident solar flux impinging a spacecraft, by blocking the view to the sun. Sunshields are commonly used for spacecraft thermal control, although only recently on small spacecraft."(NASA, 2021, p. 191)

2.5.1.5 Radiators

Most of the heat from the spacecraft is rejected into space through radiators. Radiators can be designed in a variety of ways, such as painting the satellite structure itself, mounted on the surface or a deployable radiator. Regardless of configuration, every satellite radiator rejects heat into space infrared rays. The heat rejection rate depends on the surface temperature of the radiator, its emissivity and absorptivity.

Figure 7 – Example of a heat tube model in a CubeSat 1U

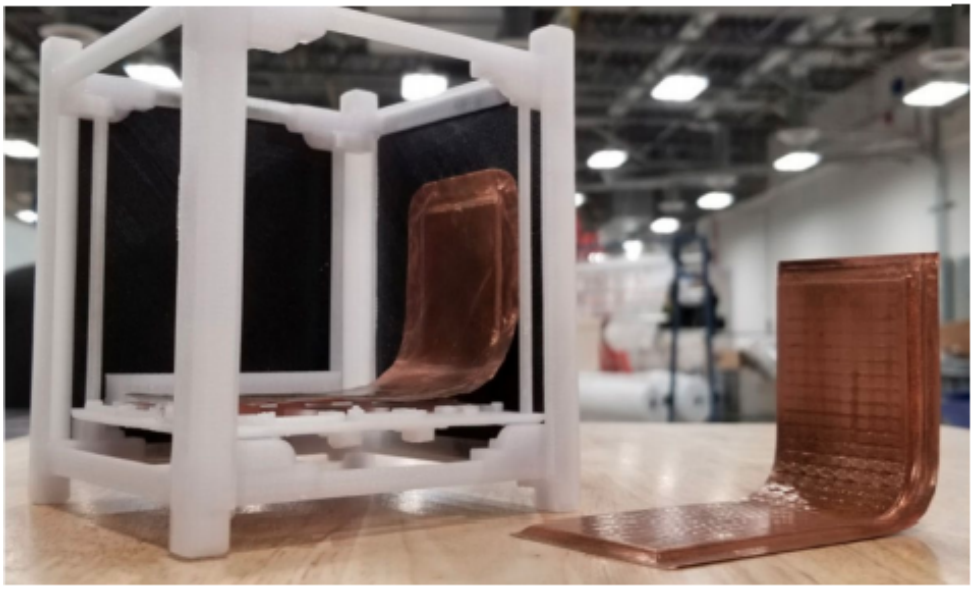

Credit: NASA (2021, p. 193).

Radiators not only need to expel the heat generated by the spacecraft but also the heat absorbed through the radiation incident on it. (GILMORE, 2002).

Body mounted radiators present a problem in Cubesats due to the limited surface area, often already occupied by solar panels, while deployable radiators also present challenges due to the internal volume limit required for their moving parts and actuators. (NASA, 2021). For a spacecraft with high power to be dissipated, as in the use case of this study, a folding radiator becomes the best alternative. In addition, alternatives with passive implantation are absent from the need for actuators such as engines and pistons.

2.5.1.6 Phase Change Materials

Phase-changing materials are used as storage of thermal energy. They are usually made from a wax stored in a metal box. When the component heats, the wax changes from solid to liquid, thus absorbing energy. Subsequently, with the operation of the radiators and the decrease in the energy emitted by the component, the wax returns to its initial state, releasing stored heat into space or back into the spacecraft. This type thermal control is indicated for cyclic energy loads that have time sufficient for the cooling of the material. Its application in Cubesats is very limited due to the high volume and mass that this component occupies in the spacecraft. (NASA, 2021).

2.5.1.7 Thermal Louvers

Thermal louvers are thermally activated blinds that regulate heat that the surface can dissipate. As the louvers open, the average emissivity of the surface changes,

changing how much heat the surface dissipates. The louvers of larger satellites have high efficacy for thermal control, however, the integration in Cubesats is challenging. (NASA, 2021).

2.5.2 Active Systems

Active systems require electrical power, sensors and data control to work. However, they can be much more efficient and accurate, very useful for components with restricted thermal requirements. (HOGSTROM, 2013). Some active control methods are coolers, heaters, active heat pipes or pumps, thermal switches, and dewars.

2.5.2.1 Electrical Heaters

Heaters are the simplest form of active thermal control, in small spacecrafts are almost always Kapton's heaters, made from a film with sewn copper circuits that heat up when applying a current. Typically come with an adhesive layer on one side for easy installation and are normally used to keep the battery within its operational temperatures. (NASA, 2021).

2.5.2.2 Cryocoolers

Cryocoolers are refrigeration devices designed to achieve temperatures of 100 Kelvin or less. Various types of cryocoolers are described by Radebaugh (2004), differentiating them by their thermal cycle or by being regenerative or recuperative. Cryocoolers are used in subsystems that require cryogenic temperatures such as spectrometers, interferometers and infrared sensors. Since these equipment only operates in very low Temperatures. (NASA, 2021). The Cubesat 6U analyzed in this work has in its list of primary components a spectrometer, however, this focuses on the study of laser dissipation, only. Several American manufacturers are in process cryocoolers for application in Cubesats.

2.5.2.3 Thermoelectric cooler (TEC)

The thermoelectric coolers have been described quite concisely by the NASA report: "A TEC is a solid-state heat pump that requires a heat exchanger to dissipate heat using the Peltier effect. During operation, current flows through the TEC to create heat transfer and a temperature differential across the ceramic substrates, causing one side of the TEC to be cold, while the other side is hot. "NASA (2021, p. 197).

2.6 METHODS OF HEAT TRANSFER ANALYSIS FOR SATELLITES

The thermal design of a spacecraft goes through several phases, being: definition of the concept and thermal requirements, validation, development, implementation and operation. In the conceptual design phase, the requirements and feasibility of the spacecraft are determined to be studied in an iterative process, until the project objectives established. In the validation phase, the conceptual design is reviewed by officers and, if approved, moves on to the hiring phase of outsourced companies for the beginning of the of the project. At this stage, all reports should be checked to avoid projects impossible to execute.

In the development phase, engineers must work together with contractors to iterate on the conceptual design and get the best thermal system design, acting on each subsystem to achieve all thermal requirements of the spacecraft as well as to draw up contingencies for various thermal scenarios during the satellite life. At this stage several components are designed and tested until a ready-made and functional spacecraft is obtained. In the deployment and operation, the spacecraft is delivered to the company contracted to launch and begins its operation in orbit. (GILMORE, 2002).

Gilmore (2002) states that an experienced engineer starts the thermal design with simplified, often hand-made analyses. Using the thermal requirements and material properties, the engineer shall draw up a Geometric Mathematical Model (GMM) and a Thermal Mathematical Model (TMM). The GMM is a mathematical model that represents the shape and position of the surfaces of the vehicle and is used to calculate form factors and radiation interactions as well as external radiation flows. The TMM is a cluster parameter representation of the capacity and thermal resistance of conduction between nodes representing points of the spacecraft and presents differential equations analogous to those of the electrical circuits. The thermal mathematical model is often done using CAD or FEM software, and then it is run several times in order to predict the most diverse operating scenarios and ensure the greatest possible understanding of the model for the project to be executed so that there is no irreparable damage during the life of the spacecraft. Gilmore (2002) still suggests some thermal analysis software: System Improved Numerical Differencing Analyzer (SINDA). as well as geometric modeling, TRASYS and NEVADA as the most widely used software.

Meseguer et al (2012) suggest ESATAN-TMS as software for spacecraft thermal analysis most widely used in Europe, in addition to mentioning others such as SINDA, Thermal Desktop, Thermica and Radsol.

Bulut e Sozbir (2015) presented an analytical nodal thermal model of a Cubesat 1U operating in a circular orbit in low Earth orbit (LEO) between 500km and 2000km and considered variation in attitude. The aim of this study was to obtain a thermal design that met the operating temperature range of electronic plates (PCBs). Bulut e Sozbir

(2015) used one node for each face of the cube, one node for each pair of solar cells (one pair per face) and one node for each PCB and consider various combinations of the relationship between the exposed aluminum area and the area of solar panels on the faces and presents graphs demonstrating the temperature variation with the altitude of the satellite, where the attitude of the satellite varies with the orbit, keeping a face always facing the planet earth. The authors conclude that a nodal analytical analysis generated satisfactory results quickly and at low cost.

Fennell (2018) did a thermal analysis of a Cubesat 6U (similar to this work) that holds as payload for an additive manufacturing experiment that generates a high waste heat (135W). The author used the Thermal Desktop software, which is integrated with AutoCAD. This software used the finite differences method in a network of nodes to calculate temperatures on each face or solid component. The component that generated the most heat is an additive manufacturing mechanism modeled as two nodes, one represents the extrusion mechanism that generates 135W of heat, and the other node represents the structure of the machine and material reservoir, which do not generate heat.

Other heat source components, of which we were considered single nodes, were electronic circuit boards (PCBs) and battery cells, which generate up to a maximum of 3W of heat each. So, Fennell (2018) performed two preliminary simulations considering the hot case, with active machine and cold case, where only the electronic components and batteries are generating heat. From the preliminary results, the author concluded that the payload should be isolated from the rest of the mli spacecraft and connected to its own radiator in order to reject maximum heat for space and not for satellite.

3 MODELING AND DESIGN

The thermal design of a spacecraft goes through several phases, being: definition of the conceptual design and thermal requirements, validation, development, implementation and operation. In this work, the conceptual design and validation of the thermal design are elaborated. The main objective of the project is that all temperatures are within the range operation for the subsystems. (GILMORE, 2002).

3.1 THERMAL DESIGN CONSIDERATIONS

The thermal system considered has four main sections: the bus, which is composed of by the main structure of the satellite and the electronic components contained therein; the Laser, which is modeled with the same thermal conductivity as aluminum and internal generation 200W heat; the radiator that is modeled as a flat plate covered with paint and the Phase Change Material (PCM) block that is modeled as a heat-absorbing mass that holds the temperature until it melts completely.

3.1.1 Design requirements

Temperature ranges have been previously determined in other NIAC papers as Franco (2018). Table 1 presented by Franco (2018) is a compilation of operational temperature data from all components of the satellite. From these, it is concluded that the range of average temperature of the satellite bus should remain between 163K to 333K (-10C to 60C) and laser should remain between 293K and 308K (20C to 35C). The temperature considered ideal for the operation of the laser will be the average temperature of the range specified by the datasheet, which is 300K (27C).

3.1.2 The CubeSat 6U

The Cubesat studied in this work is a 6U cubesat (10cm x 20cm x 30cm) composed of an aluminum structure containing the listed components in Table 1 which will remain in orbit for a period of three to six months performing experiments with Remote Laser Evaporative Molecular Absorption (R- MOTTO) Spectroscopy. The solar panels have already been scaled by Bittencourt et al (2018), six solar cells on the front of the satellite and six extended on the sides. Figure 8 presents the conceptual model of the satellite and components.

Table 1 – Operating temperature of the nanosatellite's components.

Component	Min. temperature	Max. temperature
ADCS	-10° C	60° C
Antenna System	-20° C	60° C
Batteries	-30° C	80° C
Crystal space P1U "Vasik"	-40° C	85° C
CubeSence	-10° C	70° C
Fiber coupled diode laser	20° C	35° C
Micro propulsion system	-20° C	70° C
On board computer	-25° C	65° C
Solar panels	-40° C	125° C
Spectrometer	-20° C	40° C
Structure	-40° C	80° C
Transceiver	-20° C	60° C

Credit: Franco (2018).

According to Franco (2018), a portion of solar energy that focuses on spacecraft is absorbed by solar panels and converted into electrical energy. Calculated by Equation 5:

$$Q_{elec.} = \eta \cdot Q_s \cdot A_{painel} \cdot F_{painel} \tag{5}$$

where $\eta = 0.3$ is the efficiency of the solar panel, Q_s is the solar radiation rate [W/m^2], A_{panel}, is the effective area of the panels fixed on the satellite bus (GomSpace P110 datasheet) and $F_{panel} = 1$ is the form factor for the panels. Extended panels are not part of the analysis due to the low conduction in their joints.

The Bus is modeled as a block of mass and volume equal to that of the satellite, but with uniform internal total conductivity and equal to that of the aluminium and has the energy generated by electronic equipment that generates heat. The emissivity calculated on the basis of the areas of aluminium and solar cells exposed to the space environment.

According to Franco (2018), the total heat generated by electronics in the worst case is 12W, this heat can be administered with body mounted radiators or Thermal Louvers because of this, the internal heat generation of the Bus is neglected

3.1.3 The Laser Experiment

The main mission of the spacecraft object of this study is to conduct tests and demonstrate the feasibility of Remote Laser Evaporative Molecular Absorption (R-LEMA) Spectroscopy. Cubesat's laser heats a distant spot in a material sample simulating that

Figure 8 – Model of the conceptual design for the Cubesat 6U. On the left, a isometric view of the spacecraft with the standard configuration without a PCM. On the right, an underside view detailing the PCM configuration with a heat pipe connecting it to the radiator (Appendix D).

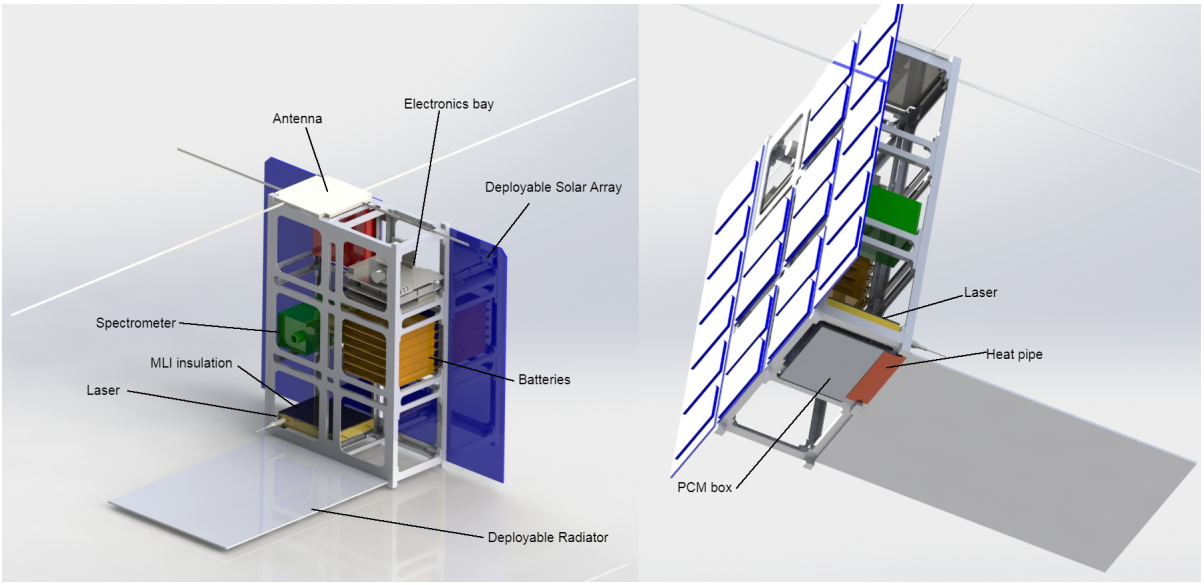

Credit: Author (2022).

of an asteroid. The infrared light emitted by the heated point passes through the cloud of vaporized molecules and is analyzed by the spectrometer to determine the molecular composition of the target sample. (HUGHES; LUBIN, 2017). The laser chosen to equip the Cubesat is the Element E18 model produced by nLIGHT. According to its datasheet (Annex A) this equipment has a heat to be dissipated of 198 Watts, which for the purpose of simplification, 200W will be adopted.

As a mission data, it is stipulated that for each experiment operation, the laser is triggered for 20 seconds, resulting in a total heat of ≈ 4000 Joules. The lower surface of the laser is considered a radiator with a coating of emissivity $\varepsilon = 0.9$ and is exposed to space. The other surfaces are insulated with Multi Layer Insulation and thermal tapes in order to isolate this component from the electronics. The only form of heat exchange considered between the laser and the Cubesat Bus is by conduction through the screws and flanges.

3.1.4 Simulated Space Environment

Hengeveld (2018) proposes a graph for easy inspection and initial sizing for Cubesats radiators (Figure 9) determining the area thermal radiators as function of the desired temperature and power to be dissipated. In this graph, the author considered that the emissivity of the radiator is 0.9.

From the data in Figure 9, for a $0.06m^2$ radiator, when the desired temperature is $300K$, its radiation capacity is $25W$. The heat generation studied in this work is

$20[s] \cdot 200[W] = 4000[J]$, so the total heat, divided by the dissipation power of the radiator, provides us with an approximate cooling time (Equation 6):

$$t = \frac{4000[J]}{25[W]} = 160[s] \tag{6}$$

Where t is the theoretical cooling time (2min 40s), without taking into account the thermal masses of the equipment and the influence of internal conduction and radiation resistances.

Considering that the mission orbit specified by Prof. Gary Hughes and the NIAC project has an orbital period of approximately 95 minutes, a 3-minute laser cooling takes only 3% of the orbital period, making it a simplification point for the problem. So in this work, the variation of albedo, planetary irradiation and solar irradiation will be neglected and the space environment has constant behavior.

Figure 9 – Ideal Radiator Areas (0 to $2m^2$) with $\varepsilon = 0.9$ as a Function of Power and Temperature

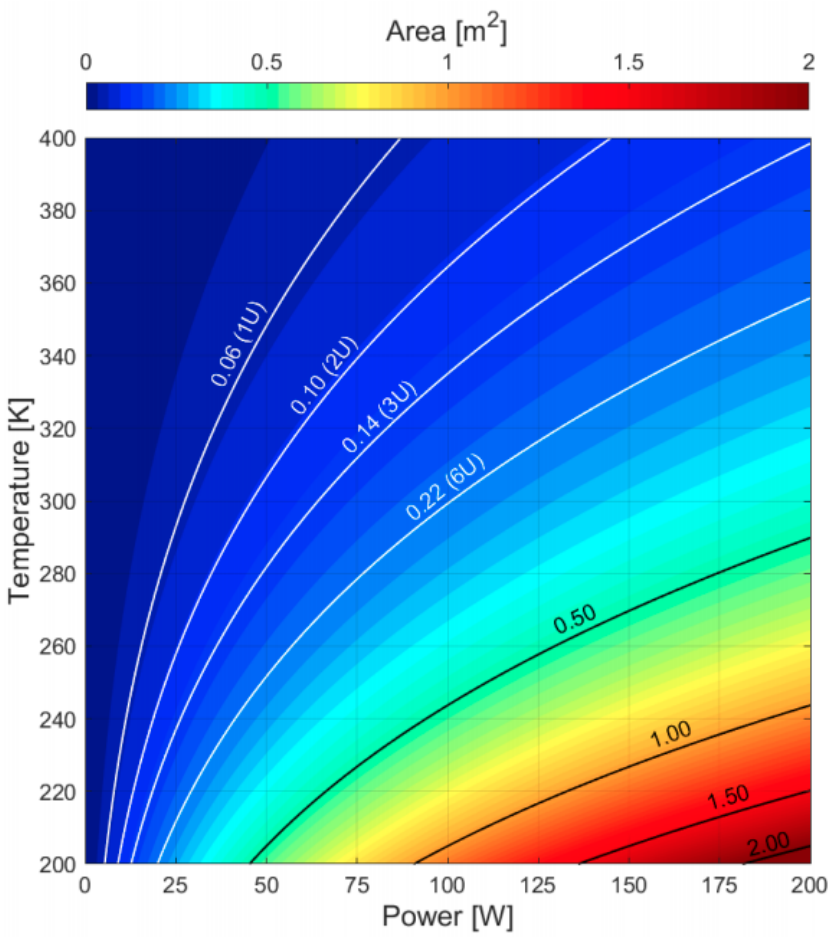

Credit: Hengeveld (2018, p. 3).

3.1.5 The Radiator

Radiator is modeled as a 2D flat plate with uniform surface temperature and total emission to the space (no back heating to the spacecraft). The rate of heat emitted by radiation is calculated by Equation 7:

$$Q_{rad,out} = \varepsilon_{we}\sigma A_{rad} \cdot (T_{rad}^4 - T_{vac}^4) \tag{7}$$

Where $\varepsilon = 0.9$ is the emissivity of white epoxy ink, σ is stefan-boltzmann's constant, T_{laser} and T_{vac} are the laser and cosmic microwave background temperatures. For an area of 0.06 square meters, the above equation results in 24.8 W, which matches the result obtained by Hengeveld (2018) using similar hypotheses.

3.2 MODELING THE THERMAL SYSTEMS

3.2.1 Heat transfer on the spacecraft

In heat transfer analysis, some bodies behave like lumped systems whose internal temperature is considered uniform during the phenomenon. The temperature varies only as a function of $T(t)$, this methodology is known as analysis of lumped parameter systems and allows great simplification of problems. When this analysis is done considering several lumped masses interacting with each other, it is known as node analysis. (ÇENGEL; GHAJAR, 2009).

During a time interval dt the body temperature varies dT, the energy balance in a time interval is given by Equation 8:

$$\sum \dot{Q} = mc\frac{dT}{dt} \tag{8}$$

The sum of the $\dot{Q}$ heat tranfers rate encompasses all forms of heat acquisition or loss by conduction, radiation, or heat generated within the control volume represented by a lumped system node. In the Equation 8, m represents the mass in $[kg]$ of the node and c the thermal capacity in $[J/kg \cdot K]$. The heat transfer rate for a satellite can be understood from Figure 2 and Equation 9:

$$mc\frac{dT}{dt} = \dot{Q}_{solar} + \dot{Q}_{albedo} + \dot{Q}_{planetIR} + \dot{Q}_{gen} + \dot{Q}_{rad,out} \tag{9}$$

Where $\dot{Q}_{gen}$ is the heat generated within the element, $\dot{Q}_{rad,out}$ is heat lost by radiation. $\dot{Q}_{solar}$ is solar radiation that directly hits the satellite element, and is calculated based on the total solar radiation rate $\dot{Q}_s = 1367[]W/m^2$ by Equation 10:

$$\dot{Q}_{solar} = -\dot{Q}_s * A_i * \varepsilon_i * \cos(\beta) \tag{10}$$

Where A_i is the node area, ε_i is the emissivity of it and β is the angle of incidence of the sun. As a simplifying hypothesis, the heat tranfers rate by albedo and planetary irradiation are constant and obtained from mean values presented by Gilmore (2002) and were obtained through the Table shown in Figure 10:

$$\dot{Q}_{albedo} = -\varepsilon_i \cdot A_i \cdot \alpha_{albedo} \cdot Q_s * F_a \tag{11}$$

$$\dot{Q}_{planetIR} = -\varepsilon_i \cdot A_i \cdot Q_{IR} \cdot F_a \tag{12}$$

Where α_{albedo} is 0.22and Q_{IR} is 274 [W/m²] from table on Figure 10 correspondent to a orbital inclination between 30 and 60 degrees. The form factor F_a is considered 1 for the purpose of simplification and obtaining a more conservative result.

The generated heat rates are fixed for the laser ($\dot{Q}_{gen,laser} = 200W$) and for the satellite bus ($\dot{Q}_{gen,bus} = 0W$) and radiation rates are modeled as described in the section 3.1.5.

Figure 10 – Earth IR and Albedo, 3.3-σ Values for Hot Case

Surface Sensitivity	Time Period	Inclination (deg)					
		0–30		30–60		60–90	
		Albedo	IR (W/m^2)	Albedo	IR (W/m^2)	Albedo	IR (W/m^2)
Albedo	16 sec	0.43	182	0.48	180	0.50	180
	128 sec	0.42	181	0.47	180	0.49	184
	896 sec	0.37	219	0.36	192	0.35	202
	30 min	0.33	219	0.34	205	0.33	204
	90 min	0.28	237	0.31	204	0.28	214
	6 h	0.23	248	0.31	212	0.27	218
	24 h	0.22	251	0.28	224	0.24	224
IR	16 sec	0.22	331	0.21	332	0.22	332
	128 sec	0.22	326	0.22	331	0.22	331
	896 sec	0.22	318	0.22	297	0.20	294
	30 min	0.17	297	0.21	282	0.20	284
	90 min	0.20	285	0.22	274	0.22	250
	6 h	0.19	269	0.21	249	0.22	221[c]
	24 h	0.19	262	0.21	245	0.20	217[c]
Both albedo and IR	16 sec	0.30	298	0.31	267	0.32	263
	128 sec	0.29	295	0.30	265	0.31	262
	896 sec	0.28	291	0.28	258	0.28	259
	30 min	0.26	284	0.28	261	0.27	260
	90 min	0.24	275	0.26	257	0.26	244
	6 h	0.21	264	0.24	248	0.24	233
	24 h	0.20	260	0.24	247	0.23	232

Credit: Gilmore (2002, p. 27).

3.2.2 Model 1: Steady state

In order to obtain a result for comparison and for a preliminary study of the nominal condition of the nanosatellite while the laser experiment does not occur, a model in permanent regime was numerically calculated using Newton's modified method in the Engineering Equation Solver (EES) software. To obtain the model on a steady state, the term on the right side of the equation 9 becomes null (Equation 13):

$$\sum \dot{Q} = 0 \tag{13}$$

Figure 11 – Thermal Mathematical Model for the Cubesat 6U

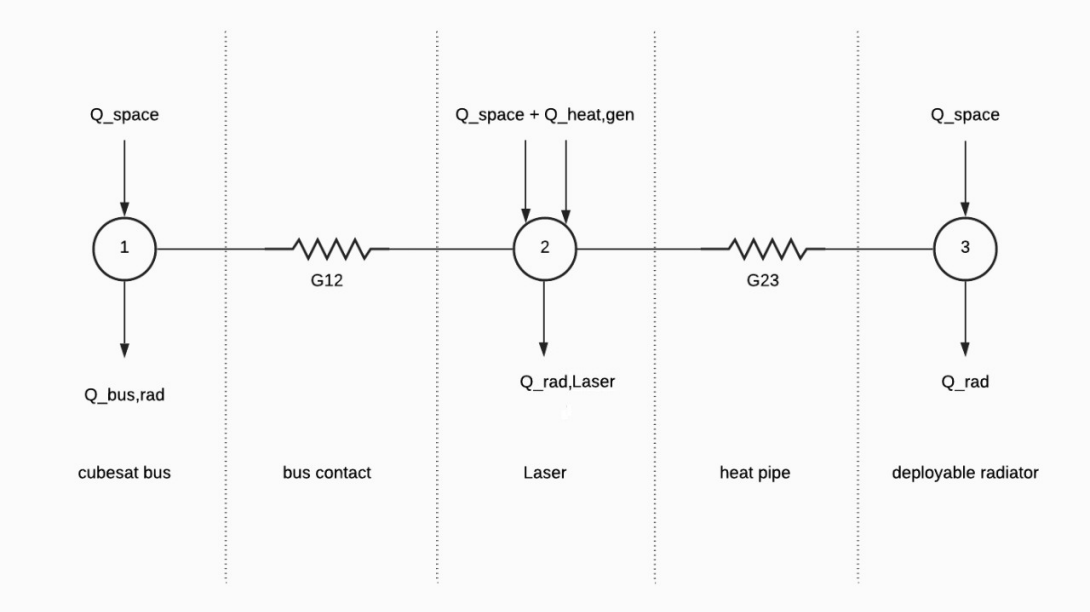

Credit: Author (2022).

Resulting in equations for the three nodes (Equation 14)(Figure 11):

$$\begin{cases} \dot{Q}_{rad,bus_out} + \dot{Q}_{space,1} - G_{1,2} * (T_2 - T_1) = 0 \\ \dot{Q}_{rad,laser,out} + \dot{Q}_{space,2} - G_{1,2} * (T_1 - T_2) - G_{2,3} * (T_3 - T_2) = 0 \\ \dot{Q}_{rad,out} + \dot{Q}_{space,3} - G_{2,3} * (T_2 - T_3) = 0 \end{cases} \tag{14}$$

where,

$$\dot{Q}_{rad,bus_out} = \varepsilon_{al} \cdot \sigma \cdot A_{bus} \cdot (T_1^4 - T_{vac}^4)$$

$$\dot{Q}_{rad,laser,out} = \varepsilon_{al} \cdot \sigma \cdot A_{laser} \cdot (T_2^4 - T_{vac}^4)$$

$$\dot{Q}_{rad,out} = \varepsilon_{al} \cdot \sigma \cdot A_{rad} \cdot (T_3^4 - T_{vac}^4)$$

$$G_{1,2} = \frac{1}{R_{bus}} = \frac{k_{al} \cdot A_f}{L}$$

$$G_{2,3} = \frac{1}{R_{pipe}}$$

Here, k_{al} is the thermal conductivity of aluminum, A_f is the area of the screw and flange that hold the Laser on the Bus. L is the distance between the Laser and the Bus. R_{pipe} is obtained through the Boyd Flexible Heat Pipe datasheet (Annex B).

The heat exchange model with regard to the space environment in the hot case is considered as a face pointing to the planet earth and receiving albedo and planetary radiation, while the other main face of the nano-satellite points to the sun, in this case solar panels are accounted for. For the cold case, the spacecraft doesn't receive heat from solar or albedo (Figure 12).

Figure 12 – Schematics of the satellite position in the models

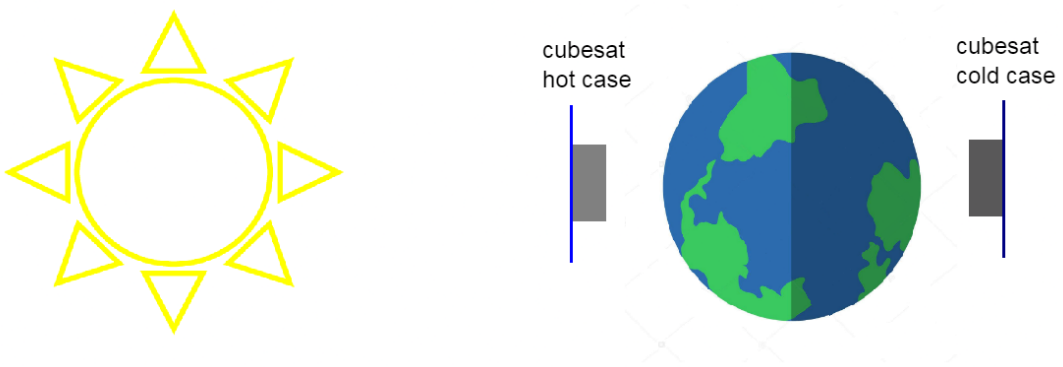

Credit: Author (2022).

3.2.3 Model 2: Transient model

TMM is a combination of design selection and support analysis. There is a large number of equipment and techniques available for the thermal design of a satellite that may or may not be included in your TMM. (GILMORE, 2002).

In this work, which is focused on the dissipation of the heat generated by the Laser, the satellite is divided into three nodes. The first represents the satellite bus with its electronic navigation and operation equipment, as well as the spectrometer, batteries and other subsystems. The second node is represented by the Laser block, with its internal heat generation in the transient period (20s). The third node is represented by the radiator and its area has been optimized according to the simulation results to meet the prerequisites. A diagram demonstrating the treatment of TMM nodes is illustrated in Figure 11.

The thermal energy balance at each node is given by Equation 15:

$$\sum \dot{Q}_i = C_i \frac{dT_i}{dt} \tag{15}$$

Where C_i is the mass times the specific heat of the material of the node.

In the transient model, one can use the forward finite differences method. The initial temperatures are given from the calculation in the model on a steady state regime, so new temperature at the node is calculated at each time step Δt successively following Equation 16:

$$\Delta T_i = \frac{\Delta t}{C_i} \sum \dot{Q}_i \tag{16}$$

And the temperature in the next step of time is given by Equation 17:

$$T_i^{+1} = T_i + \Delta T_i \tag{17}$$

The sum of the heat transfer rate at each node is detailed by Equation 18:

$$\sum \dot{Q}_i = \dot{Q}_{space,i} + \dot{Q}_{gen,i} + \dot{Q}_{cond,i-j} \tag{18}$$

Where $Q_{space,i}$ is the heat transfer rate caused by solar radiation, albedo, and planetary radiation, already demonstrated in the section 3.2.1. $Q_{gen,i}$ is the heat generation rate on node i and $Q_{cond,i-j}$ is the heat transfer rate between the i and j nodes. It is hypothesized for this work that there is no heat transfer by radiation between the nodes of the TMM. Hence, $Q_{cond,i-j}$ of node i is obtained by Equation 19:

$$\dot{Q}_{cond,i-j} = \sum_j G_{i,j} \cdot (T_j - T_i) \tag{19}$$

Where $G_{i,j}$ is the conductance of contact between i and j, T_j is the temperature of the adjacent node and T_i the temperature of the node. The conductance is obtained from the inverse of the thermal resistance of the heat pipe that connects the radiator to the laser, where A is the contact area (bolt and washer) of the laser with the Bus and k is the thermal conductivity of aluminium. Finally, the complete equation for a transient calculation time step of each TMM node is (Equation 20):

$$\Delta T_i = \frac{\Delta t}{C_i} \cdot \left(\dot{Q}_{i,j} + \dot{Q}_{space,i} + \dot{Q}_{gen,i} + \dot{Q}_{rad,out} \right) \tag{20}$$

Or more detailed at Equation 21:

$$\begin{aligned} \Delta T_i = \frac{\Delta t}{C_i} \cdot \Bigg(& \sum_j G_{i,j} \cdot (T_j - T_i) - \varepsilon_i \cdot A_i \cdot \alpha_{albedo} \cdot Q_s \\ & - \dot{Q}_s * A_i * \varepsilon_i * \cos(\beta) - \varepsilon_i \cdot A_i \cdot Q_{IR} - \dot{Q}_{gen,i} + \varepsilon_{we} \sigma A_i \cdot (T_i^4 - T_{vac}^4) \Bigg) \end{aligned} \tag{21}$$

From an initial value for the temperature of each of the nodes and a range of given time, the above equations result in the temperature distribution of each node over time as proposed in Figure 13.

Figure 13 – Flowchart of the Finite Difference Method for the transient model

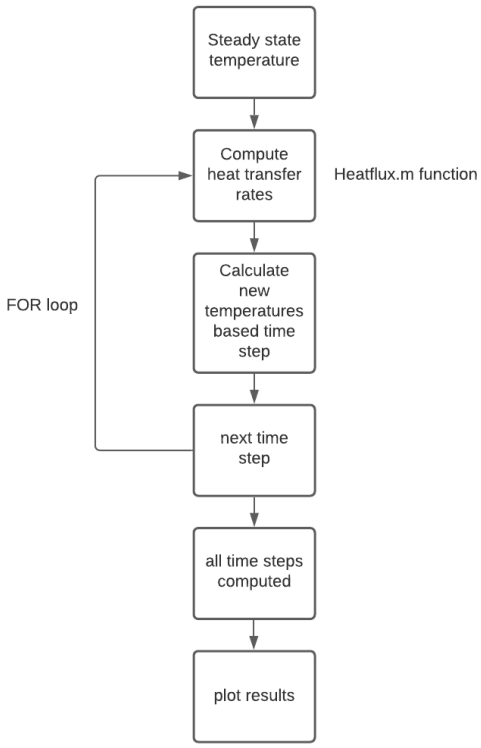

Credit: Author (2022).

3.2.4 Model 3: Transient Model with PCM

The Laser chosen by the project organizers is nLIGHT Element 18. This component has the lowest operating temperature range (20C to 35C) which is very different from the other components, so the use of a Phase Change Material was considered. The component has been modeled as an additional node to the system, is adjacent to the laser and covers the entire area that is exposed to the space environment (Figures 14 and 8). The PCM acts as a cover of the laser face, so it receives all the space radiation that the laser receives in the three-node model. In summary, in this model, the laser node is split in two, one is the laser (heat generation) and the other is the PCM (heat dissipation and storage).

In addition, the PCM acts with high conductance between itself and the laser (2x a of the heat tube). Its conductance in relation to the radiator is considered the same between the Laser and the radiator in the previous model (that is the heat pipe conductance). In summary, the PCM is modeled as one of the laser faces, which changes phase according to the melting temperature of the material. The best material

for pcm is the one that has a melting point close to 27C, the target temperature for the laser device adopted in this work.

Figure 14 – Side view of laser mount without (a) and with PCM (b)

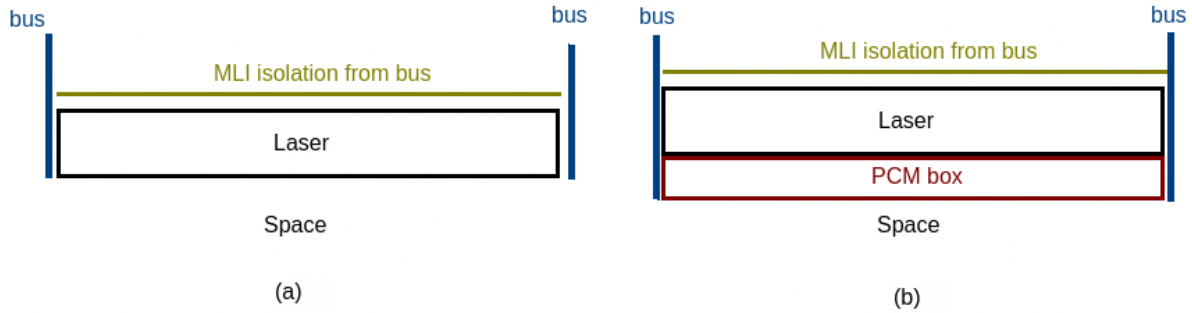

Credit: Author (2022).

3.3 THERMAL MATHEMATICAL MODEL SUMMARY

The Table 2 displays the property values considered on each node and the heat throughput values coming from the space environment calculated based on what is described in the 3.2.1 section. In the appendix A, the script 'fdm 1.m' displays the calculations in this table. The conductivity in all nodes is considered to be the Aluminium, except the radiator which has the same as copper.

Table 2 – Node proprieties

Node	Conductivity	Emissivity	Effective Area [m^2]	Q_{space} [W]	mass [kg]
1. Bus	230 [W/(m.K)]	0.82	0.06	-20.1	5
2. Laser	230 [W/(m.K)]	0.82	0.01	-9	0.51
3. Radiator	401 [W/(m.K)]	0.90	0.06	-20.4	1kg

Credit: Author (2022)

In all models, the radiator is conected to the rest of the system (laser or PCM) by a heat pipe with conducance of $37.5W/K$ (Table 3).

Table 3 – Node conduction

Node	Conductance [W/K]
$G_{laser,rad}$ or $G_{pcm,rad}$	37.5
$G_{laser,pcm}$	80
$G_{laser,bus}$	11.5

Credit: Author (2022)

4 RESULTS AND ANALYSIS

The development of the work was done based on two main analyses. The first considers 6U Cubesat without computing the internal heat exchange of the satellite bus and without using PCM, the second is a similar analysis, but the PCM was considered as a TMM node.

4.1 MODEL 1: STEADY STATE

Equation 14 solution was obtained from the Engineering Equation Solver software, using Newton's method. The steady state temperature for the satellite in a constant space environment, in the hot case, with one main face facing the earth and another towards the sun is approximately 297.6 Kelvin (24.6 C) in all three nodes. Table 4 shows the output of the EES software for the Equation 14 solution.

Table 4 – Steady State results

Node	Hot Case [K]	Cold Case [K]
1. Bus	297	293.8
2. Laser	297.6	294
3. Radiator	297.6	293.9

Credit: Author (2022)

4.2 MODEL 2: TRANSIENT MODEL

In order to determine the main unknown variables of the objective of this work, which are the peak temperature and the time required for laser to cool during and after the R-LEMA experiment, a numerical simulation by the explicit method of finite differences. In the case of the explicit method, the temperatures of the previous step or the initial temperatures are used to calculate the heat transfer rates, which in turn are used to calculate the new temperatures for the next instant of time t. (ÇENGEL; GHAJAR, 2009). In this case, Equations 15 and 16 are applied to all nodes and at every moment of simulation time.

Figure 15 – Three-node simulation result between 0 and 5 minutes

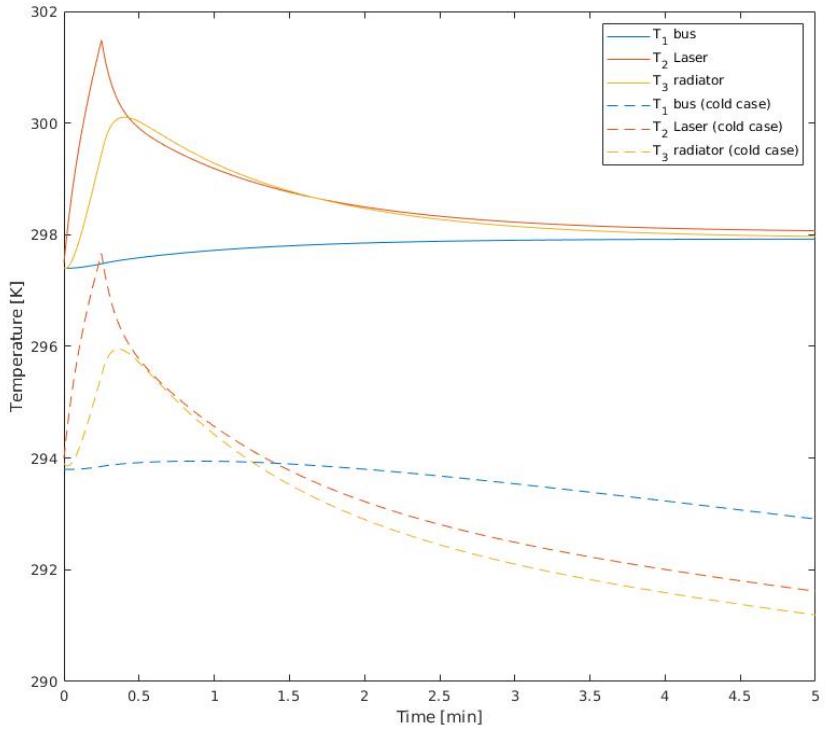

Credit: Author (2022).

The calculation of the thermal masses is done by $C_i = m_i \cdot c_i$, where the mass of the satellite bus is 3kg, the mass of the Laser is 0.51kg and the radiator mass is 1kg. The thermal capacities are 900 [J/kg K] for laser and bus 390 [J/kg K] for the radiator. All internal conductivity in nodes are considered infinte, so, each node has only one average internal temperature.

By obtaining the two equations resulting from the energy balance in the three nodes and considering the internal laser generation of 200W by the initial 20 seconds of simulation, the solution is given by an integration in a time interval of 0 to 5 minutes and another from 0 to 90 minutes (approximate period of an orbit) and initials $T_1(0) = T_2(0) = T_3(0) = 297.5K$. The result is shown in the figures 15 and 16.

Figure 15 illustrates the temperature variation of the three nodes after laser activation. The temperature of the equipment is the first to rise, up to $301.5K$ in 20 seconds, when the laser turns off, its temperature begins to drop and the radiator's temperature increases due to heat pipe conduction. It is noted that the temperature of the components drops to 298.5K in less than 5 minutes (Appendix B). Also in Figure 15 the temperature rise for the cold case ($Q_{solar} = Q_{albedo} = 0$) is denoted by the dashed lines.

Figure 16 illustrates the result of the same simulation for a 90-minute interval, which is approximately that of an orbit. It indicates that the temperature of the Cubesat

6U should normalize and become more susceptible to external variations than that of the laser experiment in less than a orbit around the earth. It is noteworthy that the simulation is done with the hypothesis of a constant space environment along the orbit, that is, the effect of additional cooling in the eclipse period is disregarded.

Figure 16 – Three-node simulation result between 0 and 90 minutes

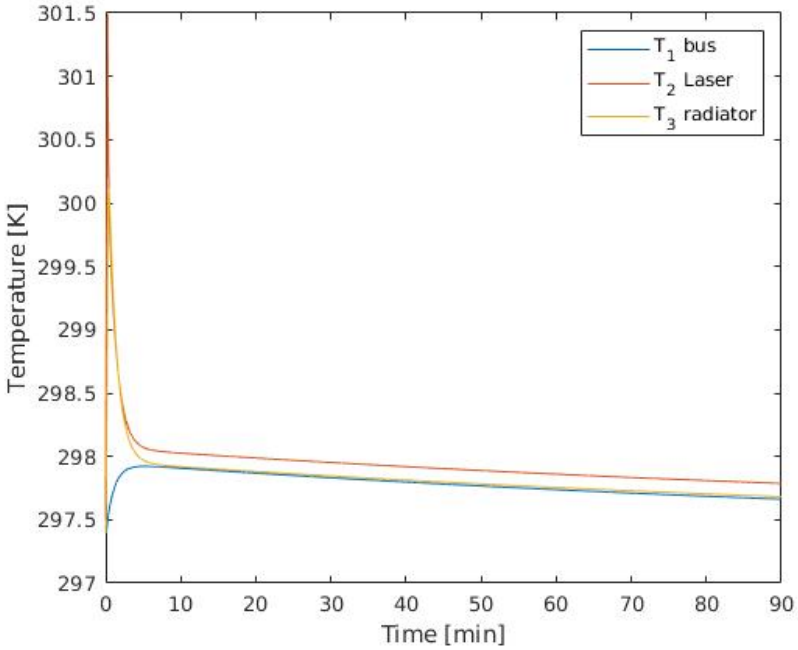

Credit: Author (2022).

4.3 MODEL 3: TRANSIENT MODEL WITH PCM

In order to ensure that the temperature of the laser device does not exceed the limits of the specifications, a Phase Change Material (PCM) block can be used in conjunction with the Laser assembly - heat tube - radiator. There is a wide variety of materials that can be used as PCM, the table 5 points out some materials considered for this application and the properties useful for the thermal mathematical model.

Table 5 – PCM materials

Material	Melting Point [K]	Heat of Fusion [kJ/kg]
Polyethylene glycol	293-298	146
Glycerol	291	199
Calcium Chloride	302	170
n-Tetradecane	279	228
n-Hexadecane	290	237
n-Heptadecane	295	213
n-Octadecane	301	244

Credit: Author (2022)

The PCM is modeled as an additional node to the previously proposed system, however, this node is adjacent to the Laser and forms a protection between the laser and the space environment. The node of the system that models the laser only has one heat source, which is the internal generation, while the PCM takes the role of interface with space. For mounting on the laser, the PCM is designed as an aluminum case with the same surface area as the laser and height of 2cm and volume of $200cm^3$ (Figure 14). The selection of the material becomes challenging for this scenario, since the temperature variation of the laser, even when there is no PCM fixed, is only 4 degrees Kelvin. The PCM box contains 100g of the selected material: Polyethylene glycol.

Due to the heat of fusion, PCM absorbs heat without varying the temperature until all the melting heat is absorbed. The total melting heat required to melt it is given by: $Q_{tot} = m_{pcm} \cdot L_{pcm}$. Where L is the heat of fusion and m the mass of the material. During transient model simulation, the total energy stored in the PCM is computed on a curve (Figure 18) and the node temperature is kept constant until all the energy required for total material fusion is absorbed. The PCM cooling and solidification model is done analogously. That is, the pcm temperature is only below the melting temperature after all the latent heat energy is returned to the satellite or expelled into the space environment. The temperature of the initial condition was set by calculating for permanent regime with the laser turned off by the EES software.

Figure 17 – Four-node simulation result between 0 and 10 minutes

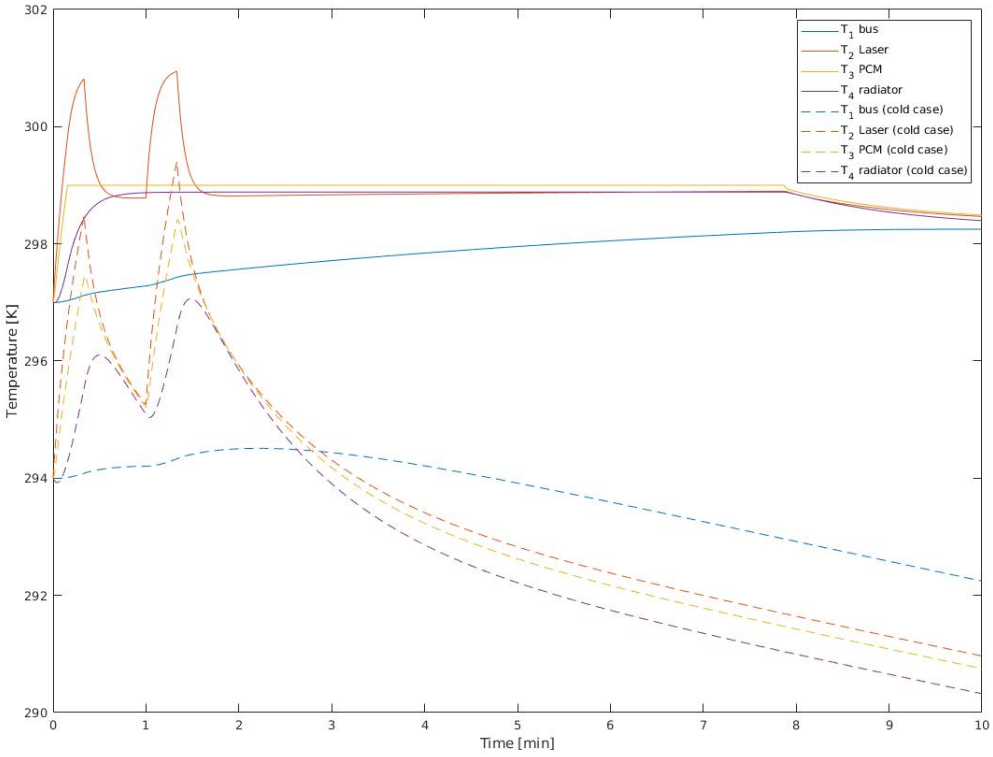

Credit: Author (2022).

Figure 17 shows the simulation result when considering laser heat generation for 20 seconds twice with a 40s interval and a total simulation time of 10 minutes fr the hot and cold ($Q_{solar} = Q_{albedo} = 0$) cases . It is noted that in the hot case the laser heats up to a temperature of 299.2K, slightly above the 299K adopted as melting temperature, and remains stable due to the polymer fusion process. When the laser is shut down at t=20, the temperature of the laser decreases and equals that of the PCM, the radiator temperature also tends to be the same as that of the PCM until all the heat of fusion is rejected into space. Finally, after 2.5 minutes, all melting heat is dissipated and the temperatures of the nodes begin to decay. The laser temperature stabilizes 0.2K above the melting temperature adopted due to losses by contact thermal resistance ($G_{2.3}$). The thermal resistance of contact adopted between the laser and the PCM box is equal to half of the thermal resistance of the heat pipe that connects the PCM to the radiator, this hypothesis was raised due to the PCM being in direct contact with the Laser and having integrated interface. The temperature of node 1 (Bus) is the slowest due to the insulation between the laser and the Bus and the small contact area where there is conduction. While in the cold case, the laser experiments don't even melt the PCM.

Figure 18 – PCM heat of fusion buildup

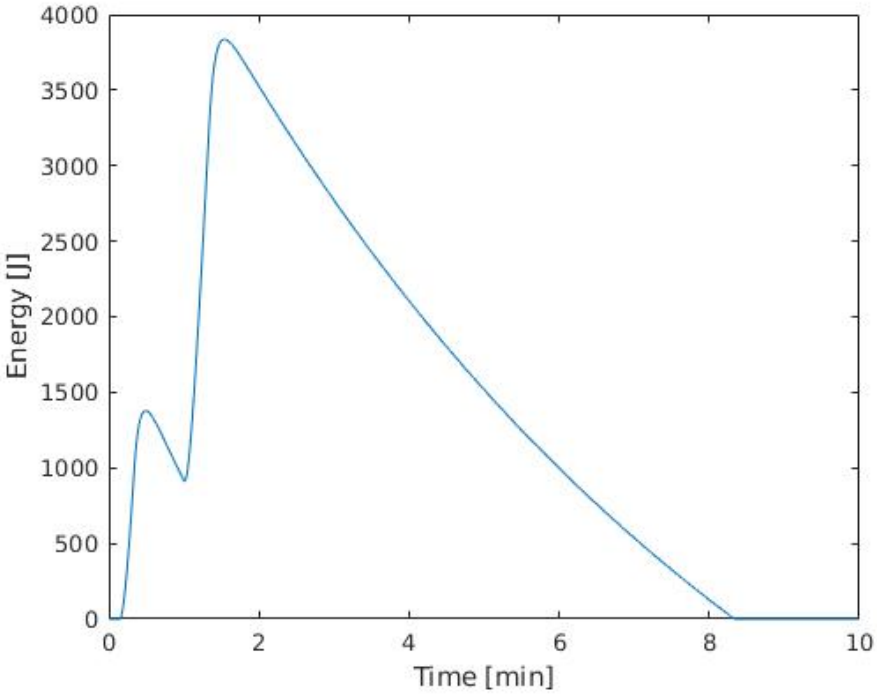

Credit: Author (2022).

Figure 18 shows the variation of heat of fusion in the phase change material. It is noticed in the graph that the PCM absorbs 1900J of heat of fusion until the instant of 20 seconds, when the laser is deactivated. After 20 seconds, the PCM begins to reject heat into the environment through the radiator until all its fusion energy is consumed and making it solid again.

Figure 19 illustrates a 90-minute simulation, it is visible that the PCM has done the work of keeping temperatures at approximately 299K, but that a quantity of heat has been absorbed by it causing it to remain in a phase change state for much longer (10 minutes) and that a full orbit is not enough to bring the temperatures to the same as of the initial condition of the simulation (Appendix C).

4.4 THERMAL CONTROL ASSESSMENTS

Based on the data from previous sections of this chapter, it is concluded that a 0.06m² radiator is enough to keep the laser cool and allow it to be used at least once per orbit, however, the use of the Phase Change Material block is an interesting solution, especially if the NIAC project is interested in performing consecutive tests without cooling time. The PCM alternative also demonstrated that although this technique allows more than one R-LEMA laser test per orbit, it will take longer to dissipate all the heat generated by the operation.

Figure 19 – Four-node simulation result between 0 and 90 minutes

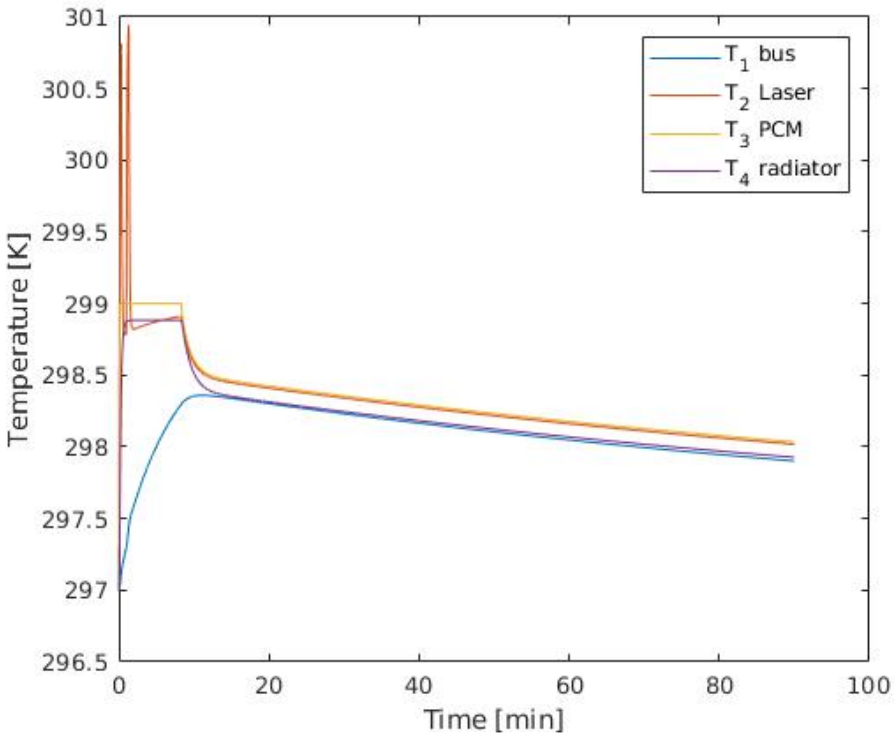

Credit: Author (2022).

During this work, the details related to heat exchanges between each face of the Bus and the components it contains were not considered, also the internal heat generation of the electrical components was disregarded. This indicates that the satellite may require another body mounted radiator or thermal louvers to administer the heat generated on the electronics bay.

5 CONCLUSIONS

The present work analyzed the variation of internal average temperatures of a Cubesat 6U in a mission of Remote Laser Evaporative Molecular Absorption (R-LEMA) Spectroscopy. Several simplifying hypotheses were considered, the most significant being that the space environment behaves constantly. Another important simplification hypothesis was that the Satellite Bus has a single internal average temperature, generating imperfections in the model, however, the central objective of the work was not to create a perfect model of the satellite, but rather to develop a preliminary thermal model of a high power laser and alternatives for the thermal control.

Three thermal control devices were used in the simulations: the radiator, the Phase Change Material (PCM) box and the heat pipe to transfer heat from the laser to the radiator. Two configurations were simulated, one with only radiator and the other with radiator and PCM. Both solutions are satisfactory for the purposes of the NIAC-sponsored project.

One configuration included a radiator and the other a radiator atached to a PCM via heat pipe. The PCM configuration shows that it can hold the temperature close to its melting point temperature and absorb the waste heat from several experiment runs in a row, while the radiator needs approximately 90 minutes to cool down the system.

5.1 RECOMMENDATIONS FOR FUTURE WORK

The simplifications adopted in this work can be explored in more detail, for example, one hypothesis that can be added to the simulation of this work is that the conditions of the space environment vary within the orbit, that is, with time. This hypothesis can be implemented in the MATLAB script since the variables $Q_{space,i}$ are no longer constant and vary over time.

Another improvement for future work would be the implementation of more nodes to the system of equations. Model each face of the satellite and also each component as individual nodes. In addition, the specification of detailed thermal properties of each component, connection, fixation and interface of the components need to be determined. Only then can a real real satellite simulation be performed.

REFERENCES

BULUT, M.; SOZBIR, N. Analytical investigation of a nanosatellite panel surface temperatures for different altitudes and panel combinations. **Applied Thermal Engineering**, v. 75, n. 1, p. 1076–1083, jan. 2015.

FENNELL, T. W. **Thermal Management Design of a 6U CubeSat with a High-Power Additive Manufacturing Payload Using Analytical Modeling with Experimental Validation**. Thesis for Master of Science degree — Florida Institute of Technology, 2018.

FINCKENOR, M. **Multilayer Insulation Material Guidelines**. Final Report — Marshall Space Flight Center, 1999.

FIXSEN, D. J. The temperature of the cosmic microwave background. **The Astrophysical Journal**, v. 707, n. 2, p. 916–920, dez. 2009.

FRANCO, G. B. H. . G. L. D. . L. F. O. R. . J. H. G. . D. L. G. . K. V. P. . B. M. Thermal control analysis on a 6u cubesat equipped with a high-power laser. **Society of Photo-Optical Instrumentation Engineers**, v. 10769, n. 1, p. 1–14, 2018.

GILMORE, D. G. **The space environment and its effects on space systems**. 2. ed. Reston, VA: American Institute of Aeronautics and Astronautics, 2002.

HEIDT, H. et al. Cubesat: A new generation of picosatellite for education and industry low-cost space experimentation. 2000.

HENGEVELD, J. A. M. . S. C. L. . D. W. Enabling high-power smallsats with advanced thermal management. **International Conference on Environmental Systems**, p. 1–11, jul. 2018.

HUGHES, G. B.; LUBIN, P. **Molecular composition analysis of distant targets.** Final Report — NASA Innovative Advanced Concepts (NIAC), 2017.

MESEGUER, J.; PEREZ GRANDE, I.; SANZ ANDRES, A. **Spacecraft thermal control**. Philadelphia, PA: Woodhead Publishing, 2012.

NASA. **State-of-the-Art Small Spacecraft Technology**. Moffett Field, California, 2021. Disponível em: https://www.nasa.gov/smallsat-institute/sst-soa.

PISACANE, V. L. **Spacecraft thermal control handbook, Volume I: Fundamental Technologies**. Reston, VA: American Institute of Aeronautics and Astronautics, 2008.

ÇENGEL, Y. A.; GHAJAR, A. J. **Tranferência de calor e massa**. 4. ed. São Paulo: McGraw Hill, 2009.

APPENDIX A - FDM_1.M

On the next page there is the script fdm 1.m

Table of Contents


```
clc
clear
```

Body heat resistance

The heat resistance due to the conduction between the laser and the bus is:

```
L= 0.01;        % m^2      bolt length
A_f = 0.0005;   % m^2      area of contact flange and bolt
k_al = 230;     % [W/mk]   aluminium conductivity

R_bus = L/(k_al*A_f);
G12 = 1/R_bus; % contact to structure condutance
```

datasheet (Boyd copper-water heat pipe)

The heat pipe resistance is obtained by dividing the max temperature difference by the nominal operating heat transfer. (placeholder estimation)

```
R_pipe = 4/150; % [K/W] heat pipe resistance
G23 = 1/R_pipe; % heat pipe condutance
```

bus emmitance heat flux to space (node 1)

```
sigma = 5.67e-8;  % [W/m2·K4] Stefan–Boltzmann constant.
T_vac = 3;        % temperature of microwave background
T_bus = 300;      % temperature of bus surface (initial guess)
E_al = 0.82;      % emissivity Anodized aluminum:

A_bus = 0.2*0.3;

Q_radbus_out = E_al*sigma*A_bus*(T_bus^4 - T_vac^4);
```

laser emmitance heat flux to space (node 2)

```
T_laser = 300;      % temperature of bus surface (initial guess)
E_al = 0.82;        % emissivity Anodized aluminum:
A_laser = 0.1*0.1;  % area of laser mount exposed to space
```

```
Q_radlaser_out = E_al*sigma*A_laser*(T_laser^4 - T_vac^4);
```

radiator heat flux (node 3)

```
T_rad = 300;            % temperature of radiator surface (initial
 guess)
E_we = 0.92;            % emissivity of white epoxy paint
A_rad = 4*.1*.1;        % radiator has surface area of two 1U sides

Q_rad_out = E_we*sigma*A_rad*(T_rad^4 - T_vac^4);
```

Q_space

```
beta = 67;        % [deg]
Q_s = 1367;       % [W/m2]
albedo = 0.22;    % [adm] Gilmore (2002) p. 26    valor medio de
 albedo
Q_IR = 274;       % [W/m2] Gilmore (2002) p. 26   valor medio de IR
Fa = 1;

A_painel = 0.006 * 6;  % area of body mounted painels in m2
eta = 0.7;

% nó 1 (bus)
Q_solar_1 = -Q_s*A_bus*E_al*cosd(beta) + Q_s*A_painel*eta;
Q_albedo_1 = -E_al*A_bus*albedo*Q_s*Fa;
Q_planet_1 = -Q_IR*A_bus*E_al;

Q_space_1 = Q_solar_1 + Q_albedo_1 + Q_planet_1

% nó 2 (laser)
Q_solar_2 = -Q_s*A_laser*E_al*cosd(beta);
Q_albedo_2 = -E_al*A_laser*albedo*Q_s*Fa;
Q_planet_2 = -Q_IR*A_laser*E_al;

Q_space_2 = Q_solar_2 + Q_albedo_2 + Q_planet_2

% nó 3 (radiator)
Q_solar_3 = -Q_s*(A_rad/2)*E_we*cosd(beta);
Q_albedo_3 = -E_we*(A_rad/2)*albedo*Q_s*Fa;
Q_planet_3 = -Q_IR*(A_rad/2)*E_we;

Q_space_3 = Q_solar_3 + Q_albedo_3 + Q_planet_3


Q_space_1 =

  -20.1080


Q_space_2 =
```

```
   -9.0927

Q_space_3 =

  -20.4032
```

Published with MATLAB® R2018a

APPENDIX B - FDM_NOPCM.M

On the next page there is the script fdm nopcm.m

```
clc
close all

C_al = 900;   % [J/kg K]
C_cu = 390;

T = [297.4 297.5 297.4];
Th = T;
dt = 1;
t = 0:dt:5*60;

% heat mass
m1 = 5;
m2 = 0.51;
m3 = 1;
C = [ m1*C_al m2*C_al m3*C_cu ];



for i = t

    if i ~= 0

        [Q] = heatflux1(T,i);
        DT = Q*dt./C;
        T = T+DT;

        Th = [Th ; T];
        %disp('--------')
    end

end



% plot
figure('position',[100 200  800 800])
plot(t/60,Th(:,1))
hold on
plot(t/60,Th(:,2))
plot(t/60,Th(:,3))
legend('T_1 bus','T_2 Laser','T_3 radiator','Location','NorthEast')
xlabel('Time [min]')
ylabel('Temperature [K]')


function [Q] = heatflux1(Tn,t)
%HEATFLUX1 Summary of this function goes here
%   Detailed explanation goes here

sigma = 5.67e-8;
```

```
T_vac = 3;

T_1 = Tn(1);
T_2 = Tn(2);
T_3 = Tn(3);


Q_space_1 =-19.3;
Q_space_2 =-9;
Q_space_3 =-20.1;

Q_gen = -200;    % must be negative
if t > 15
    Q_gen = 0;
end


%"bus heat resistance"
L= 0.01;
A_f = 0.0005;
k_al = 230;
R_bus = L/(k_al*A_f);
G12 = 1/R_bus;

%"pipe heat resistance"
R_pipe = 4/150;
G23 = 1/R_pipe;

% nó 1
E_al = 0.82;
A_bus = .2*.3;
Q_elec = -1;

Q_radbus_out = E_al*sigma*A_bus*(T_1^4 - T_vac^4);
q_1 = G12*(T_2-T_1);
Q1 = -q_1 + Q_radbus_out  + Q_space_1 + Q_elec;


% nó 2
A_laser = 0.1*0.1;

Q_radlaser_out = E_al*sigma*A_laser*(T_2^4 - T_vac^4);

q_2 = G12*(T_1-T_2) + G23*(T_3-T_2);
Q2 = -q_2 + Q_radlaser_out + Q_space_2 + Q_gen;

% nó 3
E_we = 0.9;
A_rad = 6*.1*.1;

Q_rad_out = E_we*sigma*A_rad*(T_3^4 - T_vac^4);

q_3 = G23*(T_2-T_3);
Q3 = -q_3  + Q_rad_out   + Q_space_3;
```

```
% new temperatures
Q = -[Q1 Q2 Q3];
end
```

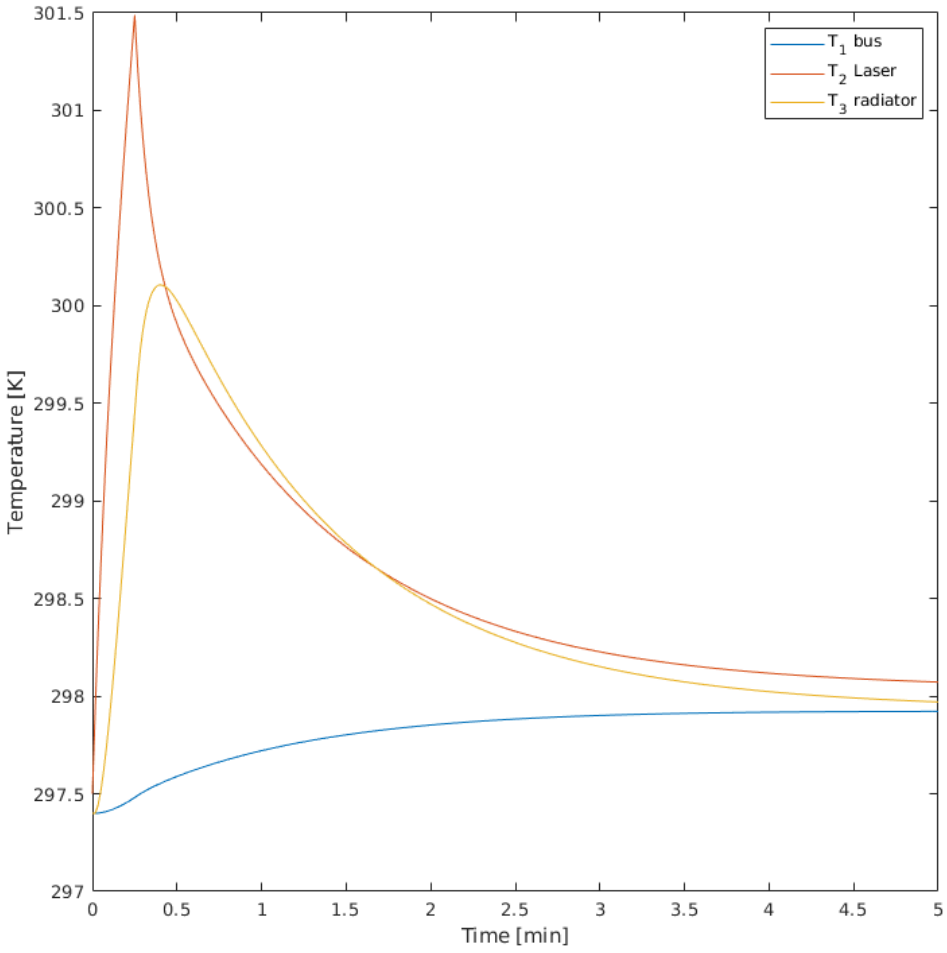

Published with MATLAB® R2018a

APPENDIX C - FDM_WPCM.M

On the next page there is the script fdm wpcm.m

```
clc
clear
close all

C_al = 900;   % [J/kg K]
C_cu = 390;
C_pcm = 900;  % polyehylene glycol

T = [297 297 297 297];
Th = T;
dt = .1;
t = 0:dt:90*60;


% heat mass
m1 = 5;
m2 = 0.51;
m3 = 0.1;
m4 = 1;
C = [ m1*C_al m2*C_al m3*C_pcm m4*C_cu ];

% pcm
L_pcm = 146000;    % [J/kg]  heat of fusion polyethilene glycol
T_pcm = 299;       % [K] melting point
Emax_pcm = m3*L_pcm;
E_pcm = 0;
Eplot = 0;
n_pcm = 3; %nede where the pcm is

if T(n_pcm) > T_pcm   % check if is already melted by the initial
 conditions
   E_pcm = Emax_pcm;
end

% integrate
for i = t

    if i ~= 0

        [Q] = heatflux2(T,i);
        DT = Q*dt./C;
        T = T+DT;

        % pcm calculations:
        % solid to liquid
        if T(n_pcm) > T_pcm && E_pcm < Emax_pcm
            T(n_pcm) = T_pcm;
            T;
            E_pcm = E_pcm + Q(n_pcm)*dt;
        end
        % liquid to solid
        if T(n_pcm) < T_pcm && E_pcm > 0
```

```
            T(n_pcm) = T_pcm;
            T;
            E_pcm = E_pcm + Q(n_pcm)*dt;
        end
        Eplot = [Eplot E_pcm];
        Th = [Th ; T];

    end

end



% plot
figure('position',[100 200  800 800])
plot(t/60,Th(:,1))
hold on
plot(t/60,Th(:,2))
plot(t/60,Th(:,3))
plot(t/60,Th(:,4))
legend('T_1 bus','T_2 Laser','T_3 PCM','T_4
 radiator','Location','NorthEast')
xlabel('Time [min]')
ylabel('Temperature [K]')

figure
plot(t/60,Eplot)
xlabel('Time [min]')
ylabel('Energy [J]')


function [Q] = heatflux2(Tn,t)
%HEATFLUX1 Summary of this function goes here
%   Detailed explanation goes here

sigma = 5.67e-8;
T_vac = 3;

T_1 = Tn(1);
T_2 = Tn(2);
T_3 = Tn(3);
T_4 = Tn(4);


Q_space_1 =-19.3;
Q_space_3 =-9;
Q_space_4 =-20.1;

Q_gen = -200;    % must be negative
if t > 20
    Q_gen = 0;
end
if t > 60
    Q_gen = -200;
```

```
end
if t > 80
    Q_gen = 0;
end

%"bus heat condutance"
L= 0.01;
A_f = 0.0005;
k_al = 230;
R_bus = L/(k_al*A_f);
G12 = 1/R_bus;

%"pipe heat condutance"
R_pipe = 4/150;
G34 = 1/R_pipe;

% laser to pcm condutance
G23 = 800;

% nó 1
E_al = 0.82;
A_bus = .2*.3;
Q_elec = -1;

Q_radbus_out = E_al*sigma*A_bus*(T_1^4 - T_vac^4);
q_1 = G12*(T_2-T_1);
Q1 = -q_1 + Q_radbus_out  + Q_space_1 + Q_elec;


% nó 2
q_2 = G12*(T_1-T_2) + G23*(T_3-T_2);
Q2 = -q_2  + Q_gen;

% nó 3
A_laser = 0.1*0.1;
Q_radlaser_out = E_al*sigma*A_laser*(T_2^4 - T_vac^4);
q_3 = G23*(T_2-T_3) + G34*(T_4-T_3);
Q3 = -q_3 + Q_radlaser_out + Q_space_3;


% nó 4
E_we = 0.9;
A_rad = 6*.1*.1;

Q_rad_out = E_we*sigma*A_rad*(T_3^4 - T_vac^4);

q_4 = G34*(T_3-T_4);
Q4 = -q_4  + Q_rad_out   + Q_space_4;


% new temperatures

Q = -[Q1 Q2 Q3 Q4];
```

```
end
```

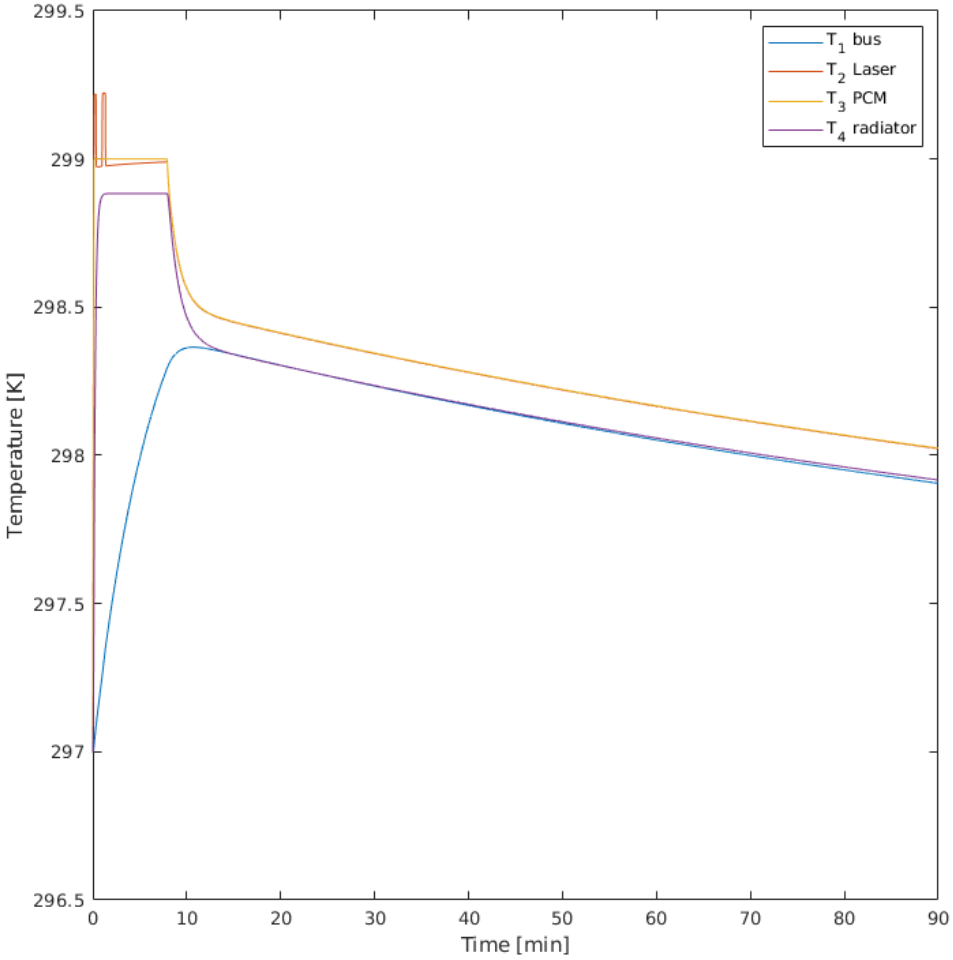
299.5
299
298.5
298
297.5
297
296.5
Temperature [K]
0
10
20
30
40
50
60
70
80
90
Time [min]
T1 bus
T2 Laser
T3 PCM
T4 radiator

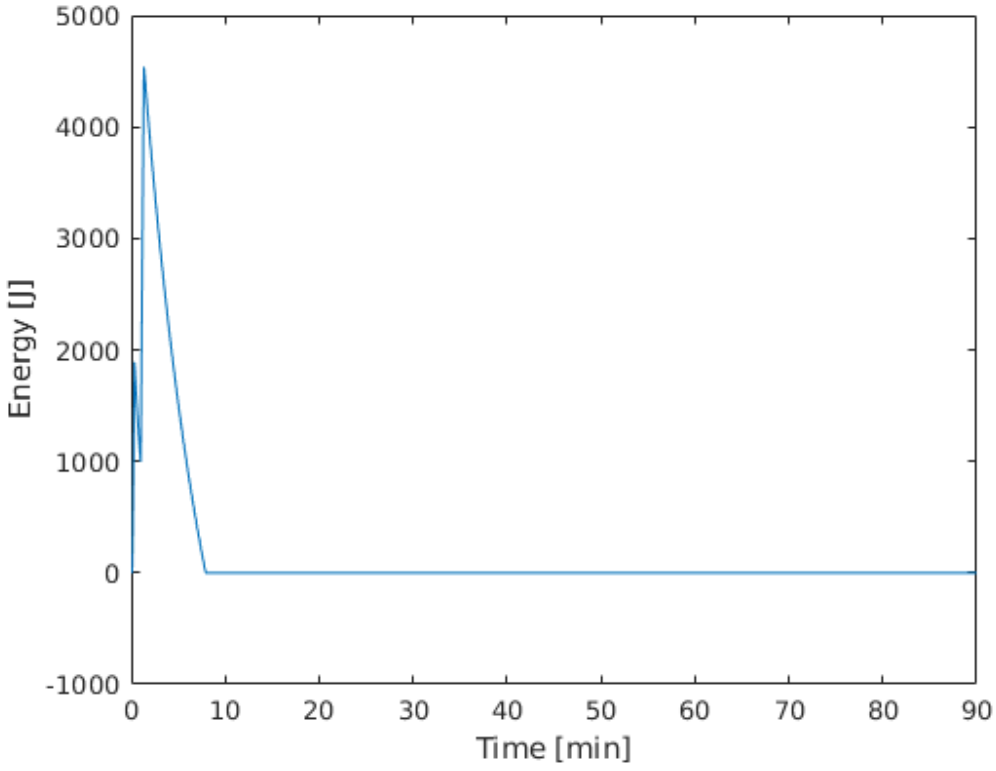

Published with MATLAB® R2018a

APPENDIX D - CONCEPTUAL RENDER

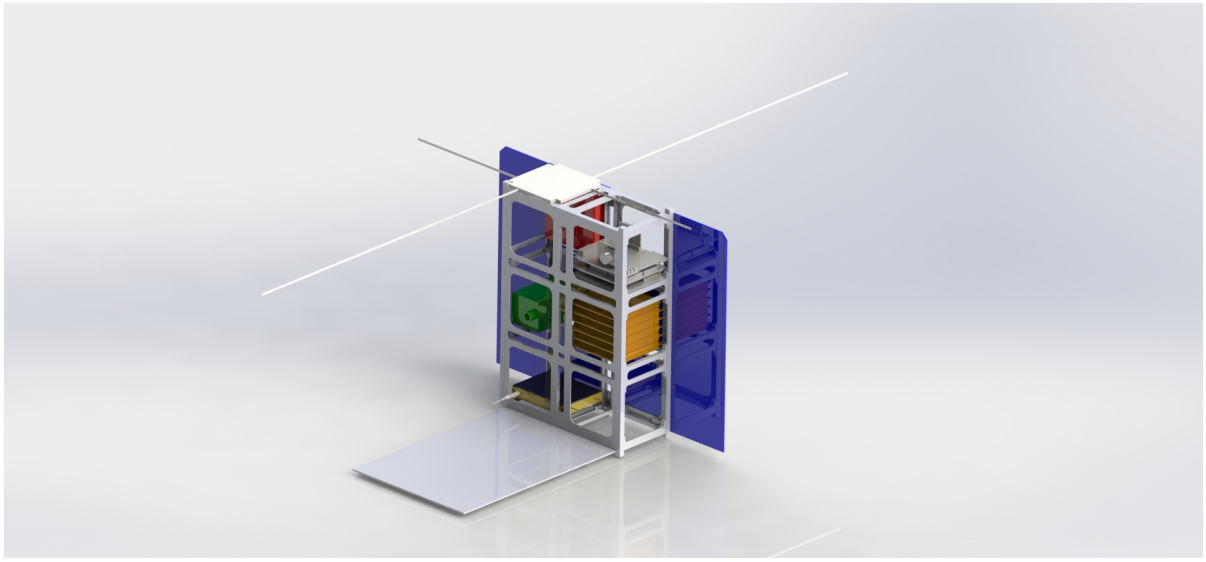

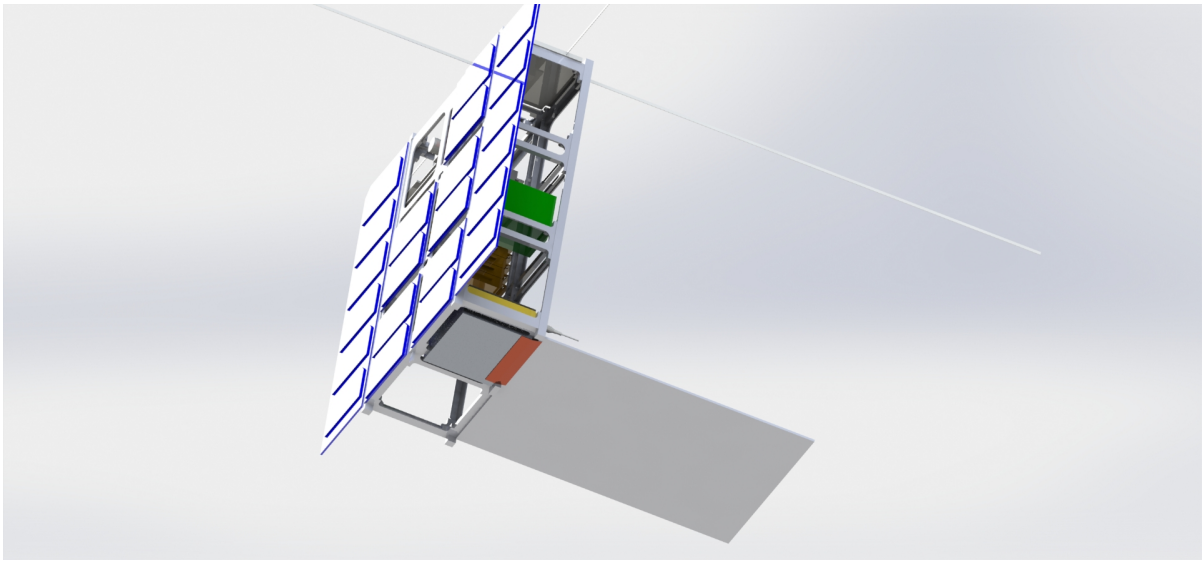

ANNEX A - NLIGHT ELEMENT® PRODUCT SPECIFICATIONS

On the next page there is the datasheet for the Laser used in this project

element®

PRODUCT SPECIFICATIONS[1]

Item Description e18-18-245-0976-7-200-0.22-SI-FPT-2.0-HT **ECCN: 6A005.d.1.b.1** [4]

Model e18.2450976200

	Units	Lower Spec	Typical	Upper Spec
Optical				
CW Output Power (in fiber)	W		245	
CW Output Power (as measured)	W	213	236	
Wavelength Centroid	nm	969.0	976.0	983.0
Spectral Width (FWHM)	nm		3.9	7.0
NA within 95% Power Enclosure	-		0.18	
Fiber Core / Clad Diameter	µm		200 / 220	
Fiber NA / Index Type	-		0.22 NA / Step Index	
Back Reflection Isolation 1030 - 1200nm	dB	15		
Electrical				
Electrical-to-Optical Efficiency	%		55	
Threshold Current	A		0.8	
Operating Current	A		16.0	16.0
Operating Voltage	V		27.7	28.3
Mechanical				
Mass	g		510	
Fiber Length	m	1.5	2.0	
Active Fiber Bend Radius	mm	35		
Fiber Jacketing	-		900 um Hytrel Loose Tube Buffer	
Fiber Termination	-		FPT	
Thermal				
Waste Heat	W		198	
Operating (Housing) Temperature [2,3]	°C		+30	
Wavelength Temperature Coefficient	nm / °C		0.35	
Wavelength Current Coefficient	nm / A		1.1	

Outline Drawing (Package Dimension 97 x 76 x 14 mm)

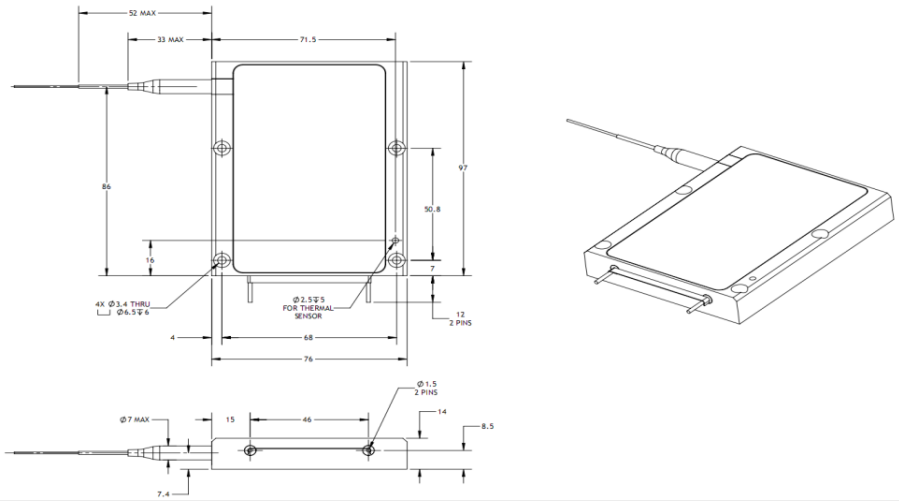

Notes

1 Production specification shown are for beginning of life performance. End of life operating current (Iop) is 110% beginning of life Iop.

2 A non-condensing environment is required for operation and storage. Storage conditions are from -20 to +70 °C with relative humidity between 5 to 85 %.

3 Operating temperature defined by the package housing.

4 Export Control Classification Number (ECCN) as defined by the Export Administration Regulations (EAR).

RoHS compliant

This product is not certified in accordance with IEC 60825-1 or 21CFR1040.10/ 21CFR1040.11 and is solely intended to be integrated into a laser product certified by the Purchaser. The Purchaser acknowledges that their product (incorporating the nLIGHT laser product) must comply with the applicable regulations before it can be sold.

VISIBLE AND/OR INVISIBLE LASER RADIATION
AVOID EYE OR SKIN EXPOSURE TO DIRECT OR SCATTERED RADIATION
CLASS 4 LASER PRODUCT

Notice
nLIGHT continually improves its products to provide customers with outstanding quality and reliability, therefore may change certain specifications and product descriptions at any time, without notice. Additionly, nLIGHT offers a limited warranty to ensure customer satisfaction. For complete details, please contact an nLIGHT sales representative.

nLIGHT

nLight Corporation
5408 NE 88th Street, Bldg E
Vancouver, Washington 98665
United States of America
Phone: 866.202.4488

ANNEX B - FLEXIBLE HEAT PIPE AND FLEXIBLE HEAT PIPE COLD PLATE DATASHEET

On the next page there is the datasheet for the Heat Pipe used in this project

BOYD CORPORATION

TECHNICAL DATA SHEET

Flexible Heat Pipe and Flexible Heat Pipe Cold Plate

For improved aerospace thermal control with a need for freedom of movement, minimum weight and maximum reliability, Aavid, Thermal Division of Boyd Corporation's custom flexible heat pipes (Figure 1) are an advanced heat pipe technology that provides an ideal solution.

These flexible heat pipes give design engineers the freedom to:

- Specify moving actuators, and remote terminals.
- Maintain thermal controls in rugged and demanding environments.
- Use as building blocks for innovative systems to meet emerging aerospace challenges.
- Vibration and isolation tested

Flexible heat pipes have been qualified for use in military aircraft — specifically, for cooling electronics on the **More Electric Aircraft**, and the **All Electric Aircraft**.

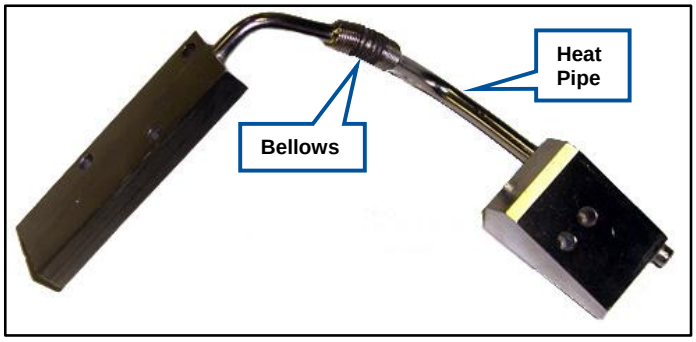

Figure 1 – Flexible Heat Pipe

Figure 2 – Flexible Heat Pipe Cold Plate

Flexible Heat Pipe Cold Plate (FHPCP)

Flexible Heat Pipe Cold Plate (FHPCP) (Figure 2), available in four configurations, solves cooling problems with a cold plate that transfers electronic heat to the most convenient heat sink via a flexible heat pipe. The flexibility allows relative motion between the heat sink and the component to be cooled — increasing durability and mean time between failures.

Key Features and Benefits

- Aircraft Level Vibration Tested: Met shock and acoustic noise design requirements, and test procedures for the aircraft equipment
- Thermal-Cycled Tested: Freeze/Thaw from -55°C to 135°C
- Bellows Flex Fatigue Tested to Over 5 million cycles with No Signs of Failure
- Shock Tested for Cooling Missile Avionics

Critical Need Application

- Vibration Isolated Heat Sources
  - » Optical Sensors
  - » Radar Amplifiers
- Assemblies that Require Relative Motion
  - » Deployable Radiators
  - » Electro-Mechanical Actuators
  - » Molding/Tooling
- Challenging “Fit-Up” with Tolerance Stack-Up Issues
  - » Complex, Multiple-Part Assemblies
  - » Difficult to Assemble, Constrained Spaces

How Can Heat Pipes Be Made Flexible?

Heat pipes are made flexible by inserting a bellows section between the evaporator heat input section, and the condenser heat output section. Flexible heat pipes are made from a wide range of metal materials, and use a variety of working fluids, depending on the application.

Flexible heat pipes can be installed in either gravity-aiding, or against-gravity orientations. The against-gravity orientation is possible because of Aavid's proprietary flexible wick structures, which are used to return the working fluid to the evaporator section. The cold plate portion attaches to the surface to be cooled, and the other end attaches to the heat sink. The flexible section allows for ease of installation, and it accommodates any relative motion between the heat source and the heat sink. The condenser region can be cooled by air cooled fins, like many other Aavid's products.

Specifications – Flexible Heat Pipe Cold Plate	
Length	Up to 30 in.
Design Power	Up to 150 Watts
Weight	Typically less than 2 lbs.
Cold Plate Size	Up to 5" x 8" x 3/16" Solid Al
Heat Sink Attachment	Customer Specified
Working Fluid	Water
ΔT at 150 Watts	Typically Less Than 4 °C